Published OnlineFirst May 18, 2010; DOI:10.1158/0008-5472.CAN-09-4210

samples and cell lines have the features of CSCs, at least in the hepatic stem cell–like HCC subtype (18). Thus, EpCAM seems to be a potentially useful marker for the isolation of liver CSCs in hepatic stem cell–like HCC.

CSCs are considered to be resistant to chemotherapy and radiotherapy (19–21), which may be associated with the recurrence of the tumor after treatment. These findings have led to the proposal of "destemming" CSCs, to induce the differentiation of CSCs into non-CSCs or to eradicate CSCs by inhibiting the signaling pathway responsible for self-renewal (22). Recent studies support this proposal and suggest the utility of bone morphogenetic proteins, activated during embryogenesis and required for differentiation of neuronal stem cells, to induce differentiation of brain CSCs and facilitate brain tumor eradication (23, 24). However, it is still debatable whether simple differentiation of CSCs effectively eradicates tumors (25).

Oncostatin M (OSM), an interleukin (IL)-6–related cytokine produced by $CD45^+$ hematopoietic cells, is known to enhance hepatocytic differentiation of hepatoblasts by inducing the activation of the signal transducer and activator of transcription 3 (STAT3) pathway (26). Although OSM, IL-6, and leukemia-inhibitory factor share STAT3 signaling cascades, OSM is known to exploit the distinct hepatocytic differentiation signaling in an OSM receptor (OSMR)–specific manner (27). In this study, we hypothesized that OSM induces hepatocytic differentiation of liver CSCs through the OSMR signaling pathway. We examined OSMR expression and the effect of OSM in $EpCAM^+$ HCC in terms of hepatocytic differentiation and antitumor activities.

Materials and Methods

Clinical HCC specimens

A total of 107 HCC tissues and adjacent noncancerous liver tissues were obtained from patients who underwent hepatectomy for HCC treatment from 1999 to 2007 in Kanazawa University Hospital. These samples were formalin-fixed and paraffin-embedded, and used for immunohistochemistry. HCC and adjacent noncancerous liver tissues were histologically diagnosed by two pathologists. An additional fresh $EpCAM^+$ AFP^+ HCC sample was obtained from a surgically resected specimen and immediately used for the preparation of single-cell suspensions and xenotransplantation. All tissue acquisition procedures were approved by the Ethics Committee and the Institutional Review Board of Kanazawa University Hospital. All patients provided written informed consent.

Cell culture and reagents

HuH1 and HuH7 cells were cultured as previously described (18). A primary HCC tissue was dissected and digested in 1 μg/mL of type 4 collagenase (Sigma-Aldrich Japan K.K.) solution at 37°C for 15 to 30 minutes. Contaminated RBC were lysed with ammonium chloride solution (STEMCELL Technologies) on ice for 5 minutes. $CD45^+$ leukocytes and Annexin V^+ apoptotic cells were removed by autoMACS-pro cell separator and magnet beads (Miltenyi Biotec K.K.). EpCAM-positive and -negative cells were enriched by autoMACS-pro cell separator and CD326 (EpCAM) MicroBeads (Miltenyi Biotec K.K.). Recombinant OSM was purchased from R&D Systems, Inc. 5-Fluorouracil (5-FU) was obtained from Kyowa Kirin.

Quantitative reverse transcription-PCR analysis

Total RNA was extracted using TRIzol (Invitrogen) according to the instructions of the manufacturer. The expression of selected genes was determined in triplicate using the 7900 Sequence Detection System (Applied Biosystems). Each sample was normalized relative to β-actin expression. Probes used were *TACSTD1*, Hs00158980_m1; *AFP*, Hs00173490_m1; *KRT19*, Hs00761767_s1; *hTERT*, Hs00162669_m1; *Bmi1*, Hs00180411_m1; *POU5F1*, Hs00999632_g1; *CYP3A4*, Hs00430021_m1; *OSMR*, Hs00384278_m1; and *ACTB*, Hs99999903_m1 (Applied Biosystems).

Western blotting

Whole cell lysates were prepared using radioimmunoprecipitation assay lysis buffer as described previously (28). Rabbit polyclonal antibodies to STAT3 (Cell Signaling Technology, Inc.), rabbit polyclonal anti-OSMR antibodies H-200 (Santa Cruz Biotechnology), mouse monoclonal anti–phosphorylated STAT3 (Tyr^{705}) antibody (3E2; Cell Signaling Technology), and mouse monoclonal anti–β-actin antibody (Sigma-Aldrich) were used. Immune complexes were visualized by enhanced chemiluminescence (Amersham Biosciences, Corp.) as described by the manufacturer.

Immunohistochemistry and immunofluorescence analyses

Immunohistochemistry was performed using Envision+ kits (DAKO) according to the instructions of the manufacturer. Anti-EpCAM monoclonal antibody, VU-1D9 (Oncogene Research Products), was used for detecting EpCAM. Goat anti-OSMR polyclonal antibodies (C-20) were obtained from Santa Cruz Biotechnology. Mouse anti-CYP3A4 polyclonal antibodies (Abnova), mouse anti–cytokeratin (CK) 19 monoclonal antibody (DAKO), and mouse anti–Ki-67 monoclonal antibody MIB-1 (DAKO) were used for detecting CYP3A4, CK19, and Ki-67, respectively. Samples with >5% positive staining in a given area for a particular antibody were considered to be positive. For immunofluorescence analyses, anti-EpCAM antibody (Oncogene Research Products), anti-gp130ST antibodies (Santa Cruz Biotechnology), and anti–phosphorylated STAT3 (Tyr^{705}) antibody (3E2; Cell Signaling Technology) were used. Alexa 488 FITC-conjugated anti-mouse IgG or Alexa 568 Texas red–conjugated anti-goat/rabbit IgG (Molecular Probes) were used as secondary antibodies. Confocal fluorescence microscopic analysis was performed essentially as previously described (18).

Fluorescence-activated cell sorting analyses

Cultured cells were trypsinized, washed, and resuspended in HBSS (Lonza) supplemented with 1% HEPES and 2% fetal bovine serum (FBS). Cells were then incubated with FITC-conjugated anti-EpCAM monoclonal antibody Clone Ber-EP4 (DAKO) on ice for 30 minutes, and analyzed using

Published OnlineFirst May 18, 2010; DOI:10.1158/0008-5472.CAN-09-4210

a FACSCalibur (BD Biosciences). Intracellular AFP, CK19, and albumin levels were examined using a BD Cytofix/Cytoperm Fixation/Permeabilization Kit (BD Biosciences), anti-AFP mouse monoclonal antibody (Nichirei Biosciences Inc.), anti-CK19 mouse monoclonal antibody (DAKO), and rabbit polyclonal anti-albumin antibodies (Cell Signaling Technology), respectively.

Cell proliferation and colony formation assay

For cell proliferation assays, 2×10^3 cells were seeded in 96-well plates and cultured with 1% FBS DMEM (control), 1% DMEM with OSM (100 ng/mL), 5-FU (2 μg/mL), or OSM (100 ng/mL) and 5-FU (2 μg/mL) for 3 to 7 days without media changes. Cell viability was evaluated in quadruplicate using a CellTiter 96 AQueous kit (Promega). For colony formation assays, 1×10^3 cells were harvested in a one-well Culture Slide (BD Biosciences) and cultured with 1% FBS DMEM (control) with or without OSM (100 ng/mL). Culture medium was replaced every 3 days and the colonies were fixed with ice-cold 100% methanol and used for immunofluorescence 10 days after the initiation of treatment.

RNA interference

SiRNAs specific to OSMR (Silencer Select siRNA S17542) and a control siRNA (Silencer Select Negative Control no. 1) were obtained from Ambion (Applied Biosystems). To each well of a six-well plate, 2×10^5 cells were seeded 12 hours before transfection. Transfection was performed using LipofectAMINE 2000 (Invitrogen), according to the instructions of the manufacturer. A total of 100 pmol/L of siRNA duplex was used for each transfection.

Apoptosis assay

Cells were cultured in 1% FBS DMEM (control), 1% FBS DMEM with OSM (100 ng/mL), 5-FU (2 μg/mL), or OSM (100 ng/mL) and 5-FU (2 μg/mL) for 3 days in six-well plates or in culture slides (BD Biosciences). Annexin V binding to cell membranes was visualized using Annexin V-FITC antibodies and a FACSCalibur flow cytometer (BD Biosciences). Activation of caspase 3 was visualized by immunohistochemistry or immunofluorescence using anti-active caspase-3 polyclonal antibodies (Promega), as described by the manufacturer.

Animal studies

Six-week-old NOD/SCID mice (NOD/NCrCRl-*Prkdc*^{scid}) were purchased from Charles River Laboratories, Inc. The protocol was approved by the Kanazawa University Animal Care and Use Committee. One million tumor cells were suspended in 200 μL of DMEM and Matrigel (1:1), and a s.c. injection was performed. The incidence and size of subcutaneous tumors were recorded. Intratumoral injections of 50 μL of PBS (control), OSM (2 μg/tumor), 5-FU (250 μg/tumor), or OSM (2 μg/tumor) and 5-FU (250 μg/tumor) were initiated twice weekly 48 days after the injection of tumor cells when the average volume of four tumors in each group had reached 400 mm^3. For histologic evaluation, tumors were formalin-fixed and paraffin-embedded.

Statistical analyses

The association of OSMR expression and clinicopathologic characteristics in HCC was examined using either Mann-Whitney U or χ^2 tests. Student's t test was used to compare various test groups assayed by quantitative reverse transcription-PCR analysis. All analyses were performed using GraphPad Prism software.

Results

Distinct expression of OSMRs in HCC

Before exploring the effect of OSM on HCC, we examined the expression of its receptor, OSMR, in surgically resected HCC and adjacent noncancerous liver tissues by immunohistochemistry. Representative staining of OSMRs in tumor/nontumor tissues is shown in Fig. 1A. In general, cell surface and cytoplasmic immunoreactivity to OSMR were rarely detected in hepatocytes in chronic hepatitis liver (a), but were frequently detected in small hepatocyte-like cells in the stroma or transitional cells in the lobule of cirrhotic liver (b), as indicated by the arrows. Note that immunoreactivity to OSMR was not detected in bile duct epithelia or ductular reactions in which EpCAM$^+$ hepatic progenitor cells are thought to accumulate (Supplementary Fig. S1), suggesting that OSMRs might be expressed in hepatic progenitor cells committed to hepatocytes. Immunoreactivity to OSMRs was more strongly detected in HCC than in noncancerous liver (c), and the expression was heterogeneous in the tumor. Of note, OSMRs were detected in HCC cells at the invasive front area of the tumor (d) where CSCs are known to invade frequently (arrows).

Immunoreactivity to OSMR antibodies and EpCAM antibodies was detected in 66 (61.7%) and 38 (35.5%) of 107 HCC specimens, respectively. The clinicopathologic characteristics of OSMR$^+$ and OSMR$^-$ HCC cases are shown in Table 1. OSMR$^+$ HCC was characterized by high serum AFP values ($P = 0.009$), poorly differentiated morphology ($P < 0.0001$), and a high frequency of EpCAM$^+$ HCCs ($P = 0.024$), suggesting that the OSMR is expressed in HCC with stem/progenitor cell features. OSMR$^+$ HCC was also characterized by young onset of disease and male dominance, although these features did not reach statistical significance ($P = 0.052$ and 0.058, respectively). OSMR was more frequently detected in EpCAM$^+$ HCCs (76.3%) than in EpCAM$^-$ HCCs (53.7%). Expression of OSMR and EpCAM was further investigated by double immunofluorescence analysis, and immunoreactivity to OSMR was detected in both EpCAM$^+$ normal hepatic progenitors (Fig. 1B) and EpCAM$^+$ HCC cells (Fig. 1C). These data suggest that although OSMR is more widely expressed than EpCAM in HCC, OSMR is frequently expressed in EpCAM$^+$ normal hepatic progenitors and liver CSCs.

OSM induces hepatocytic differentiation of EpCAM+ HCC

Because OSMR was expressed in the majority of EpCAM$^+$ HCCs, we investigated the effect of OSM on EpCAM$^+$ HCC cell lines. First, we examined the expression of OSMR and its signal transducer glycoprotein 130 (gp130) in EpCAM$^+$ AFP$^+$ HCC cell lines HuH1 and HuH7 by immunofluorescence

Published OnlineFirst May 18, 2010; DOI:10.1158/0008-5472.CAN-09-4210

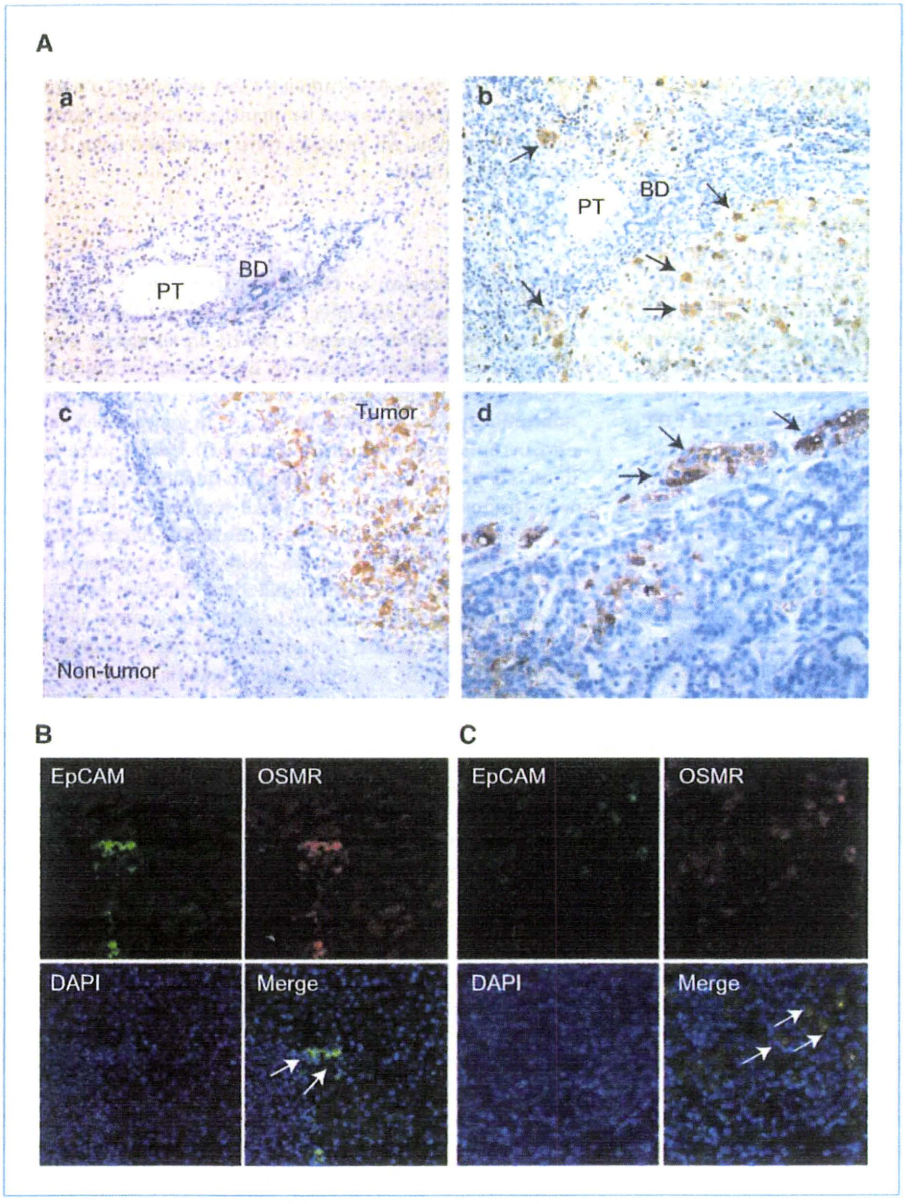

Figure 1. A, representative images of OSMR staining in noncancerous liver tissues and HCC tissues. Immunoreactivity to OSMR was not detected in hepatocytes in chronic hepatitis liver tissue (a) but was detected in a subset of small hepatocyte-like cells in the stroma or transitional cells in the lobule (b, arrows) of cirrhotic liver tissue. OSMR was more abundantly expressed in HCC than in noncancerous liver (c). OSMR$^+$ cancer cells were disseminated in the invasive front area of the tumor (d, arrows). PT, portal tract; BD, bile duct. B and C, double immunofluorescence analysis of EpCAM (green) and OSMR (red) expression in noncancerous (B) and HCC (C) tissues.

(Fig. 2A). Both gp130 and OSMR protein expressions were detected in these cells, consistent with the immunohistochemical data. Because OSM is known to induce the hepatocytic differentiation of hepatoblasts in a STAT3-dependent manner, we investigated the effect of OSM on phosphorylation of STAT3 in HuH1 and HuH7 cells by immunofluorescence and Western blotting. Incubation of HCC cells for 1 hour with OSM at a concentration of 100 ng/mL resulted in the induction and nuclear accumulation of phosphorylated STAT3 compared with controls (Fig. 2B and C). We examined the effect of OSM on the EpCAM$^+$ cell population in HuH1 and HuH7 cells. We first labeled HuH1 and HuH7 cells with CD326 (EpCAM) MicroBeads and FITC-conjugated anti-EpCAM antibodies (Clone Ber-EP4) and performed positive/negative selection using magnetic activated cell sorting to determine the appropriate gating criteria for EpCAM-high (designated as EpCAM$^+$) and EpCAM-low/negative (designated as EpCAM$^-$) cell population (Fig. 2D, top). It is interesting that OSM treatment (100 ng/mL for 72 hours) diminished the EpCAM$^+$ cell population from 50.7% to 10.1% in HuH1 and from 55.2% to 28.8% in HuH7 cells when the same constant gating criteria was applied (Fig. 2D, bottom).

We used RNA interference to investigate whether the decrease in EpCAM$^+$ cells by OSM treatment depends on the expression of OSMR. Transfection of siRNAs specific to *OSMR* (si-OSMR) resulted in the knockdown of target genes

Published OnlineFirst May 18, 2010; DOI:10.1158/0008-5472.CAN-09-4210

compared with the control (si-Control) in HuH1 and HuH7 cells 48 hours after transfection (Supplementary Fig. S2A). We further confirmed the decrease of OSMR protein expression by immunofluorescence and Western blotting 72 hours after transfection (Supplementary Fig. S2B and C). When we treated these HuH1 and HuH7 cells with OSM (100 ng/mL) for 1 hour, we observed the decrease of phosphorylated STAT3 by *OSMR* gene silencing compared with the control (Supplementary Fig. S2C). Furthermore, OSM-mediated decrease in the number of EpCAM+ cells was inhibited by *OSMR* gene silencing (Supplementary Fig. S2D), suggesting that OSM exploits the diminution of EpCAM+ cells through the activation of the OSMR signaling pathway in EpCAM+ HCC.

We further examined the effect of OSM on hepatocytic differentiation by quantitative reverse transcription-PCR and fluorescence-activated cell sorting (FACS) analyses. OSM treatment in HuH1 cells reduced the expression of hepatic progenitor–related genes including *AFP, KRT19* (encoding CK19), and *TERT* (encoding telomerase reverse transcriptase; TERT; Fig. 3A). OSM treatment further reduced the expression of *BMI1* and *POU5F1* (encoding Oct4), which is known to be expressed and required for self-renewal in embryonic stem cells. OSM treatment also increased the expression of the hepatocyte marker, *CYP3A4*. Furthermore, OSM treatment reduced AFP+ and CK19+ cells and increased albumin+ cells compared with the untreated controls, as evaluated by the geometric mean of the fluorescence intensities of whole cells analyzed by intracellular FACS (Fig. 3B). Similar results were obtained in HuH7 cells (data not shown) and, taken together, these data suggest that OSM induced the hepatocytic differentiation of EpCAM+ HCCs.

Hepatocytic differentiation of EpCAM+ HCC by OSM augments cell proliferation

In general, normal stem cells are more quiescent than differentiated cells in terms of cell division. We therefore evaluated the effect of OSM on cell proliferation in HuH1 and HuH7 cells. It is interesting that OSM treatment for 10 days resulted in a larger colony formation following treatment with OSM (100 ng/mL) compared with untreated controls. Of note, the majority of cells comprising these larger colonies were EpCAM−, or had low expression levels, whereas a subset of untreated control cells maintained high EpCAM expression (Fig. 3C). Similar results were obtained when cell proliferation was examined using a [3-(4, 5-dimethylthiazol-2-yl)-5-(3-carboxymethoxyphenyl)-2-(4-sulfophenyl)-2H-tetrazolium] tetrazolium assay and Ki-67 labeling index (Fig. 3D). OSM modestly enhanced cell proliferation (top) and increased Ki-67–positive cells (middle and bottom) compared with untreated controls in both HuH1 and HuH7 cells with statistical significance (Fig. 3D).

OSM treatment increases chemosensitivity of EpCAM+ HCC

The abovementioned data imply that although OSM may induce the hepatocytic differentiation of dormant EpCAM+ liver CSCs, OSM treatment alone might instead enhance cell proliferation through expansion of amplifying differentiated cancer cells *in vitro*, raising the question of efficacy of differentiation therapy in EpCAM+ HCC. Because rapidly amplifying cells are considered to be more sensitive to chemotherapeutic agents, we investigated the effect of combining OSM treatment with conventional chemotherapy to target both dormant CSCs and amplifying non-CSCs. We have shown that 5-FU treatment

Table 1. Clinicopathologic characteristics of OSMR+ and OSMR− HCC cases used for immunohistochemical analyses

Variables	OSMR+ (n = 66)	OSMR− (n = 41)	P*
Age (years, mean ± SE)	62.7 ± 1.3	66.4 ± 1.3	0.052
Sex (male/female)	55/11	27/14	0.058
Etiology (HBV/HCV/other)	25/35/6	8/30/3	0.10
Liver cirrhosis (yes/no)	43/23	26/15	1.0
AFP (ng/mL, mean ± SE)	6,453 ± 5901	1,039 ± 935	0.009
Histologic grade†			
I–II	3	16	
II–III	54	20	
III–IV	9	5	<0.0001
Tumor size (<3 cm/>3 cm)	30/36	15/26	0.42
Tumor-node-metastasis classification			
I/II	48	31	
III/IV	18	10	0.82
EpCAM (positive/negative)	29/37	9/32	0.024

*Mann-Whitney U test or χ^2 test.
†Edmondson-Steiner.

Published OnlineFirst May 18, 2010; DOI:10.1158/0008-5472.CAN-09-4210

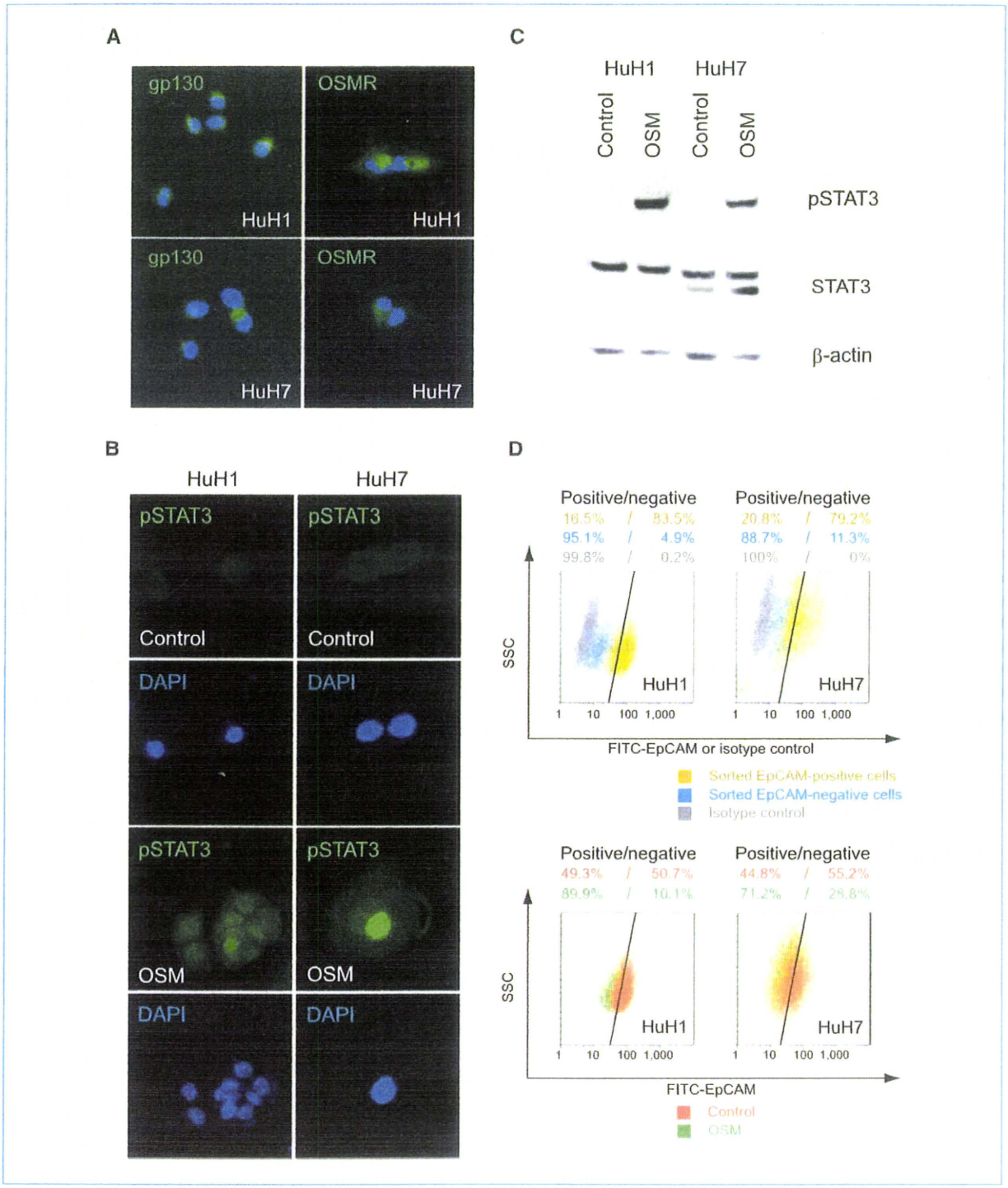

Figure 2. A, immunofluorescence analysis of gp130 and OSMR expression in HuH1 and HuH7 cell lines. B, immunofluorescence analysis of phosphorylated STAT3 expression in HuH1 and HuH7 cell lines stimulated by OSM (100 ng/mL for 1 hour) and controls. C, Western blotting analysis of whole or phosphorylated STAT3 protein expression in HuH1 and HuH7 cells stimulated by OSM (100 ng/mL for 1 hour) and controls. D, FACS analysis of HuH1 and HuH7 cells stained with FITC-conjugated anti-EpCAM antibodies. Top, EpCAM-high (designated as $EpCAM^+$; yellow) and EpCAM-low/negative cells (designated as $EpCAM^-$; blue) were enriched by magnetic activated cell sorting and labeled with FITC-conjugated anti-EpCAM antibodies or isotype control antibodies. Bottom, cells were cultured in 1% FBS DMEM with (green) or without OSM (100 ng/mL; orange) for 3 days and stained with FITC-conjugated anti-EpCAM antibodies.

Published OnlineFirst May 18, 2010; DOI:10.1158/0008-5472.CAN-09-4210

alone could diminish EpCAM- non-CSCs which results in the enrichment of EpCAM+ CSCs in HCC (18). We therefore explored the effect of 5-FU in combination with OSM on EpCAM+ HCC cell proliferation and apoptosis *in vitro*.

When HuH1 and HuH7 cells were treated with OSM alone and cultured for 7 days, cell proliferation was modestly increased compared with untreated controls (Fig. 4A). In contrast, 5-FU treatment clearly inhibited cell proliferation.

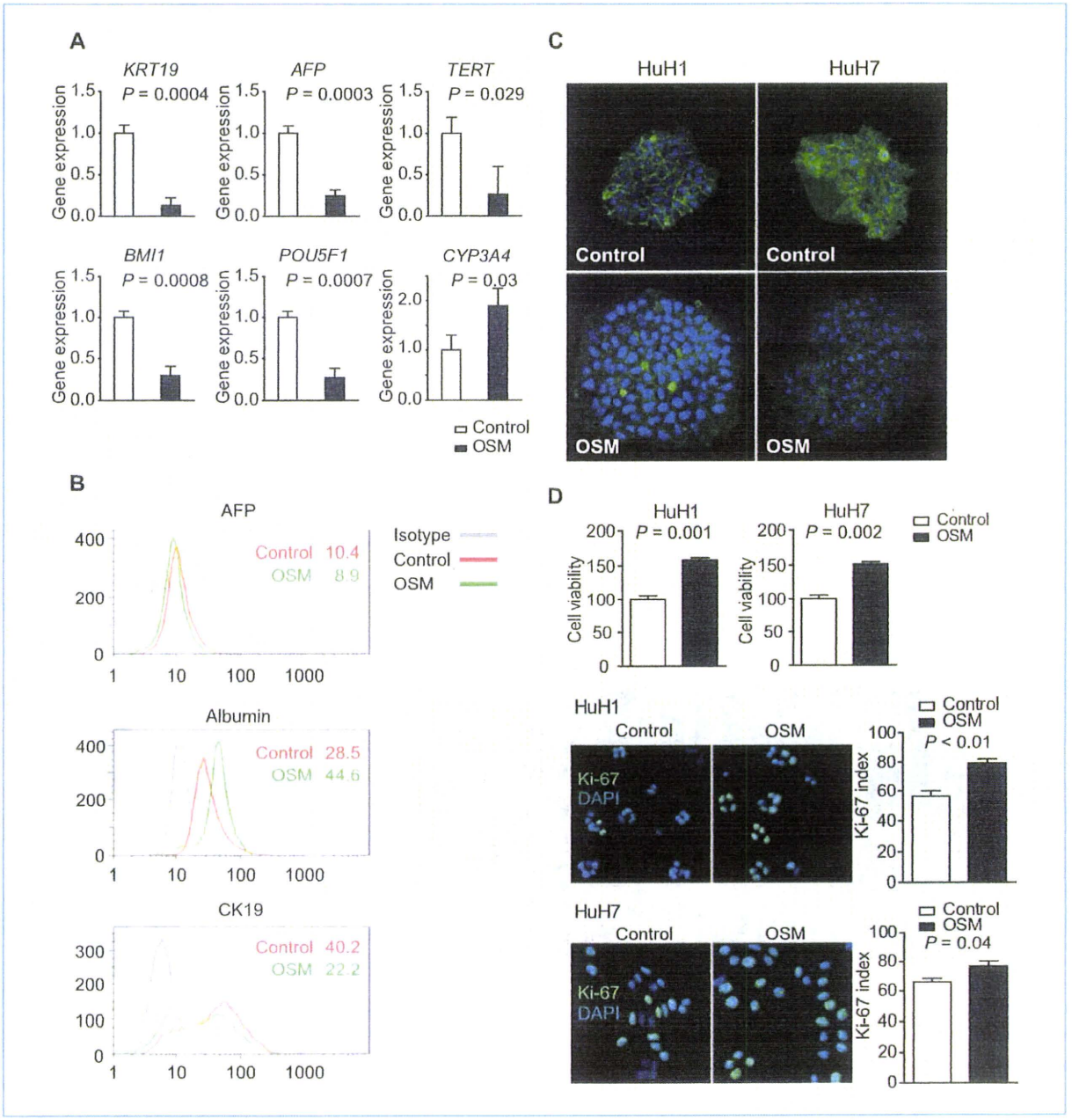

Figure 3. A, quantitative reverse transcription-PCR analysis of HuH1 cells cultured in 1% FBS DMEM with (black columns) or without (white columns) OSM (100 ng/mL) for 3 days. B, intracellular FACS analysis of HuH1 cells cultured in 1% FBS DMEM with (green line) or without (red line) OSM (100 ng/mL) for 3 days. The number in the figure indicates the geometric mean of the fluorescence intensity on a logarithmic scale. C, immunofluorescence analysis of HuH1 and HuH7 cell colonies cultured in 1% FBS DMEM with or without OSM (100 ng/mL) for 10 days. Colonies were fixed with 100% ice-cold methanol and stained with FITC-conjugated anti-EpCAM antibodies. D, top, cell proliferation assay of HuH1 and HuH7 cells cultured in 1% FBS DMEM with (black column) or without (white column) OSM (100 ng/mL) for 3 days. Middle and bottom, immunofluorescence analysis of HuH1 and HuH7 cells cultured in 1% FBS DMEM with or without OSM (100 ng/mL) for 3 days. Cells were fixed with 100% ice-cold methanol and stained with anti–Ki-67 antibodies.

Published OnlineFirst May 18, 2010; DOI:10.1158/0008-5472.CAN-09-4210

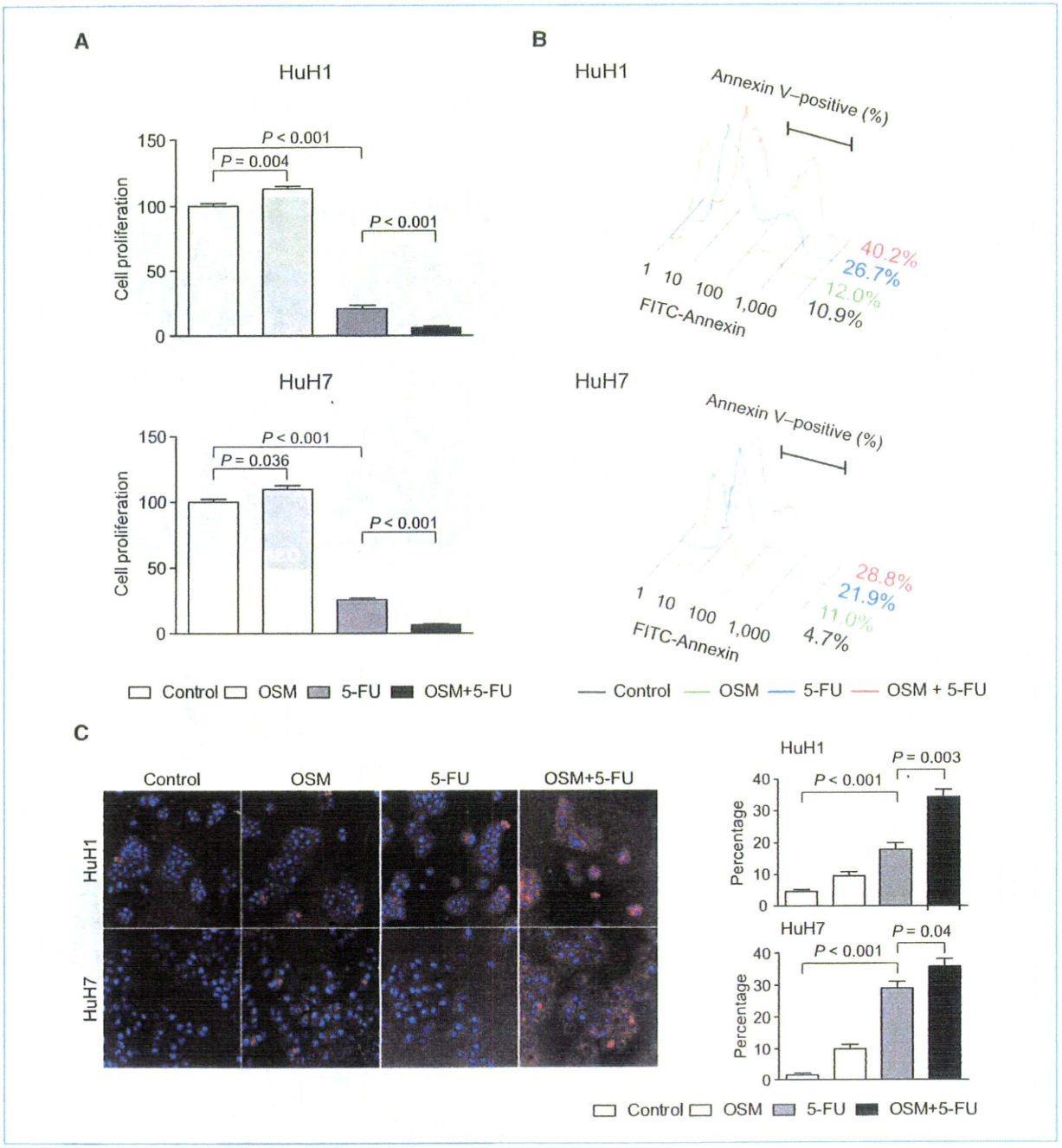

Figure 4. A, cell proliferation assay of HuH1 and HuH7 cells cultured in 1% FBS DMEM with OSM (100 ng/mL; light gray columns), 5-FU (2 μg/mL; gray columns), OSM (100 ng/mL) and 5-FU (2 μg/mL; black columns), or PBS as control (white columns) for 7 days. B, FACS analysis of HuH1 and HuH7 cells stained with FITC-conjugated anti–Annexin V antibodies. Cells were cultured in 1% FBS DMEM with OSM (100 ng/mL; green line), 5-FU (2 μg/mL; blue line), OSM (100 ng/mL) and 5-FU (2 μg/mL; red line), or PBS as control (gray line) for 3 days. C, left, immunofluorescence analysis of HuH1 and HuH7 cells stained with anti–active caspase 3 antibodies. Cells were cultured in 1% FBS DMEM with OSM (100 ng/mL), 5-FU (2 μg/mL), OSM (100 ng/mL) and 5-FU (2 μg/mL), or PBS control for 3 days. Right, bar graphs indicating the percentages of active caspase 3–positive cells.

Noticeably, the combination of OSM and 5-FU effectively suppressed cell proliferation in HuH1 and HuH7 cells (Fig. 4A). We further investigated the effects of OSM and 5-FU on apoptosis, evaluated by Annexin V binding to cell membranes and the activation of caspase 3 (Fig. 4B and C). Although OSM treatment alone had a small effect on the induction of apoptosis, 5-FU treatment induced Annexin V^+ and activated caspase 3^+ cells more than in the control. The

Published OnlineFirst May 18, 2010; DOI:10.1158/0008-5472.CAN-09-4210

combination of OSM and 5-FU most strongly induced apoptosis in both HuH1 and HuH7 cells with statistical significance.

Finally, we investigated the effect of OSM on EpCAM$^+$ HCC *in vivo* using a primary HCC specimen and cell lines. Single-cell suspensions from primary EpCAM$^+$ HCC cells (1×10^6 cells) were injected into 6-week-old male NOD/SCID mice, and these cells formed subcutaneous tumors 48 days after transplantation. Subsequently, 50 μL of PBS, OSM (2 μg/tumor), 5-FU (250 μg/tumor), or OSM (2 μg/tumor) and 5-FU (250 μg/tumor) solution were injected directly into each tumor twice a week. Although OSM treatment alone showed weak tumor-suppressive effects, the changes in tumor size showed no significant difference compared with controls (Fig. 5A). Similarly, 5-FU treatment alone showed limited tumor-suppressive effects. However, the combination of OSM with 5-FU showed a marked inhibition of tumor growth compared with PBS control or 5-FU alone ($P = 0.02$ and 0.05, respectively). Immunohistochemical analysis of xenografted tumors showed that OSM treatment decreased the number of EpCAM$^+$ or CK19$^+$ cells and increased CYP3A4$^+$ cells *in vivo* (Supplementary Fig. S3A and B). FACS analysis of xenografted tumors further confirmed the decrease of EpCAM$^+$ cell population by OSM treatment *in vivo* (Supplementary Fig. S3C). Immunohistochemical analysis revealed that the combination of OSM with 5-FU strongly induced the activation of caspase 3 compared with PBS control, OSM, or 5-FU (Fig. 5B). Taken together, these data suggest that hepatocytic differentiation of EpCAM$^+$ HCC cells induced by OSM was the most effective for inhibition of tumor growth *in vivo* when the conventional chemotherapeutic agent 5-FU was coadministered.

Discussion

A growing body of evidence suggests that there are similarities between normal stem cells and CSCs in terms of self-renewal programs (29). We have recently reported that Wnt/β-catenin signaling augments self-renewal and inhibits the differentiation of EpCAM$^+$ liver CSCs (18). In the present study, we have shown that the OSM-OSMR signaling pathway is maintained in HCCs with stem/progenitor cell features. OSM induces hepatocytic differentiation and activates cell division in dormant EpCAM$^+$ liver CSCs (Fig. 5C). Furthermore, we have shown that the combination of OSM and 5-FU effectively inhibits tumor cell growth, revealing the importance of targeting both CSCs and non-CSCs for eradication of the tumor.

OSM is a pleiotropic cytokine that belongs to the IL-6 family which includes IL-6, IL-11, and leukemia-inhibitory factor. These cytokines share the gp130 receptor subunit as a common signal transducer, and activate Janus tyrosine kinases and the STAT3 pathway. However, gp130 forms a heterodimer with a unique partner such as the IL-6 receptor, leukemia-inhibitory factor receptor, or OSMR, thus transducing a certain signaling uniquely induced by each cytokine (30). Of note, OSM is known to activate hepatocytic differentiation programs in hepatoblasts in an OSMR-specific manner (27), and our data showed that OSM could induce hepatocytic differentiation and active cell proliferation in EpCAM$^+$ HCC through OSMR signaling.

OSMR is expressed in hepatoblasts in the fetal liver (26). We have found that OSMR is frequently expressed in normal hepatic progenitors but is rarely detected in hepatocytes in adult livers. Interestingly, OSMR$^+$ HCC was characterized by

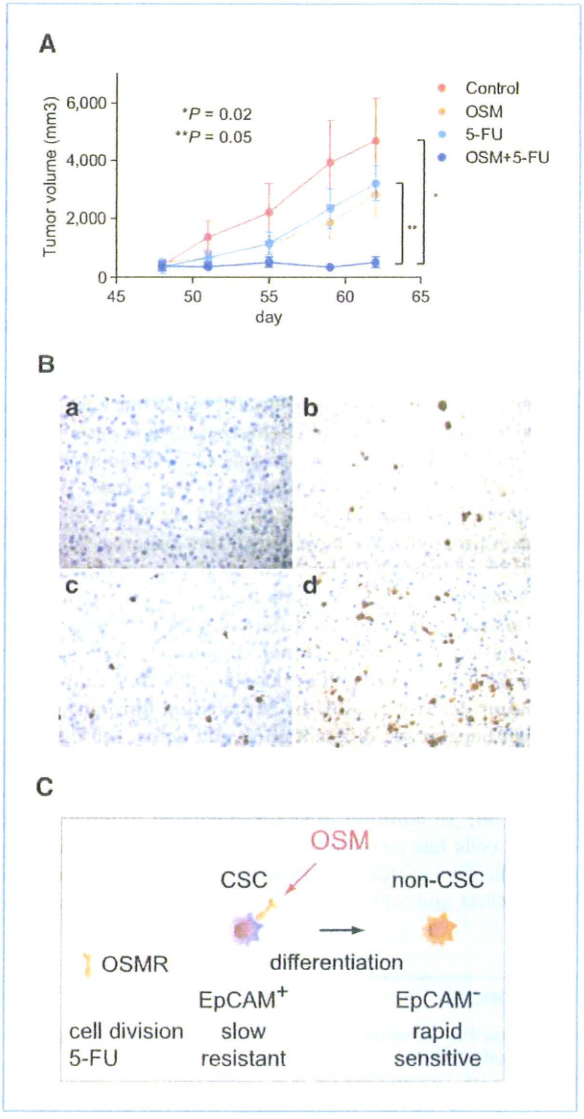

Figure 5. A, effect of PBS, OSM, 5-FU, and OSM plus 5-FU injections on the growth of primary EpCAM$^+$ AFP$^+$ HCC xenograft tumors in NOD/SCID mice ($n = 4$ in each group). Intratumoral injection of 50 μL of PBS, OSM (2 μg/tumor), 5-FU (250 μg/tumor), or OSM (2 μg/tumor) and 5-FU (250 μg/tumor) was initiated 48 days after transplantation, twice per week. B, representative images of activated caspase 3 staining of xenograft tumors in each treatment group (a, PBS; b, OSM; c, 5-FU; and d, OSM and 5-FU). C, a schematic diagram of the effect of OSM on EpCAM$^+$ liver CSCs. Dormant EpCAM$^+$ liver CSCs with OSMR expression respond to OSM and differentiate into rapidly dividing EpCAM$^-$ non-CSCs that are highly sensitive to 5-FU.

Published OnlineFirst May 18, 2010; DOI:10.1158/0008-5472.CAN-09-4210

high serum AFP, frequent EpCAM positivity, and poorly differentiated morphology, suggesting that OSMR is more likely expressed in HCC with stem/progenitor cell features (16). Although the regulatory mechanisms of OSMR are still unclear, it is plausible that OSMR expression is regulated by a signaling pathway activated during the process of hepatogenesis. Because gp130 is known to be ubiquitously expressed, regulation of OSM signaling might be largely dependent on the expression status of OSMR in normal and tumor tissues. Recent studies have shown the potential role of methylation of CpG islands located in OSMR promoter in colorectal cancer (31, 32). Clarification of OSMR promoter activity regulation, including CpG methylation, might provide clues for better understanding of hepatocytic differentiation signaling in both normal hepatic stem cells and CSCs.

It has been postulated that both normal stem cells and CSCs are dormant and show slow cell cycles. Consistent with this, CSCs are considered to be more resistant to chemotherapeutic agents than non-CSCs, possibly due to slow cell cycles as well as an increased expression of ATP-binding cassette transporters, robust DNA damage responses, and activated antiapoptotic signaling (20, 33, 34). Therefore, development of an effective strategy by targeting CSC pools together with conventional chemotherapies is essential to eradicate a tumor mass. Two strategies have been investigated to reduce the CSCs population in the tumor; that is, inhibition of self-renewal programs and activation of differentiation programs. We have shown that hepatocytic differentiation of liver CSCs by OSM results in enhanced cell proliferation *in vitro*. We have further shown here that OSM-mediated hepatocytic differentiation of liver CSCs in combination with conventional chemotherapy effectively suppresses HCC growth. It is possible that OSM may boost antitumor activity of 5-FU by "exhausting dormant CSCs" through hepatocytic differentiation and active cell division. It is encouraging that similar success with differentiation therapy has recently been reported in several cancers (24, 35, 36). In addition, HNF4-α–mediated differentiation of HCC cells has recently been reported to be effective for the eradication of HCC (37). However, although the combination of OSM and 5-FU effectively inhibited tumor growth in our model, we could not observe the shrinkage of the tumor. Thus, induction of CSC's differentiation with eradication of non-CSCs might not be enough for the eradication of the tumor, which might suggest the importance of inhibiting self-renewal as well as stimulating differentiation of CSCs. Because we induced the hepatocytic differentiation of the subcutaneous tumor by local injection of OSM, further rigorous studies are clearly required to assess the effect of OSM on liver CSCs and its utility for differentiation therapy in HCC.

CSCs may acquire resistance against differentiation therapy by additional genetic/epigenetic changes during treatment by clonal evolution, as observed in conventional chemotherapy. Indeed, it has recently been suggested that bone morphogenetic protein–mediated brain CSC differentiation failed in a subset of brain tumors in which bone morphogenetic protein receptor promoters were methylated and silenced (23). Similarly, OSMR silencing by promoter methylation might result in the development of OSM-resistant clones in HCC.

In conclusion, OSMR is expressed in certain types of HCC with stem/progenitor cell features, and OSM induces hepatocytic differentiation and active cell division of $OSMR^+$ liver CSCs to enhance chemosensitivity to 5-FU. The clinical safety and utility of OSM should be evaluated in the near future.

Disclosure of Potential Conflicts of Interest

No potential conflicts of interest were disclosed.

Acknowledgments

We thank Masayo Baba and Nami Nishiyama for excellent technical assistance.

Grant Support

Ministry of Education, Culture, Sports, Science and Technology, Japan grant-in-aid (no. 20599005).

The costs of publication of this article were defrayed in part by the payment of page charges. This article must therefore be hereby marked *advertisement* in accordance with 18 U.S.C. Section 1734 solely to indicate this fact.

Received 11/17/2009; revised 03/12/2010; accepted 03/31/2010; published OnlineFirst 05/18/2010.

References

1. Fialkow PJ. Clonal origin of human tumors. Biochim Biophys Acta 1976;458:283–321.
2. Clarke MF, Dick JE, Dirks PB, et al. Cancer stem cells—perspectives on current status and future directions: AACR Workshop on Cancer Stem Cells. Cancer Res 2006;66:9339–44.
3. Jordan CT, Guzman ML, Noble M. Cancer stem cells. N Engl J Med 2006;355:1253–61.
4. Al-Hajj M, Wicha MS, Benito-Hernandez A, Morrison SJ, Clarke MF. Prospective identification of tumorigenic breast cancer cells. Proc Natl Acad Sci U S A 2003;100:3983–8.
5. Bonnet D, Dick JE. Human acute myeloid leukemia is organized as a hierarchy that originates from a primitive hematopoietic cell. Nat Med 1997;3:730–7.
6. O'Brien CA, Pollett A, Gallinger S, Dick JE. A human colon cancer cell capable of initiating tumour growth in immunodeficient mice. Nature 2007;445:106–10.
7. Ricci-Vitiani L, Lombardi DG, Pilozzi E, et al. Identification and expansion of human colon-cancer-initiating cells. Nature 2007;445:111–5.
8. Singh SK, Hawkins C, Clarke ID, et al. Identification of human brain tumour initiating cells. Nature 2004;432:396–401.
9. Visvader JE, Lindeman GJ. Cancer stem cells in solid tumours: accumulating evidence and unresolved questions. Nat Rev Cancer 2008;8:755–68.
10. El-Serag HB, Rudolph KL. Hepatocellular carcinoma: epidemiology and molecular carcinogenesis. Gastroenterology 2007;132:2557–76.
11. Mishra L, Banker T, Murray J, et al. Liver stem cells and hepatocellular carcinoma. Hepatology 2009;49:318–29.
12. Chiba T, Kita K, Zheng YW, et al. Side population purified from hepatocellular carcinoma cells harbors cancer stem cell-like properties. Hepatology 2006;44:240–51.

Published OnlineFirst May 18, 2010; DOI:10.1158/0008-5472.CAN-09-4210

13. Ma S, Chan KW, Hu L, et al. Identification and characterization of tumorigenic liver cancer stem/progenitor cells. Gastroenterology 2007;132:2542–56.
14. Yang ZF, Ho DW, Ng MN, et al. Significance of CD90+ cancer stem cells in human liver cancer. Cancer Cell 2008;13:153–66.
15. Yang W, Yan HX, Chen L, et al. Wnt/β-catenin signaling contributes to activation of normal and tumorigenic liver progenitor cells. Cancer Res 2008;68:4287–95.
16. Yamashita T, Forgues M, Wang W, et al. EpCAM and α-fetoprotein expression defines novel prognostic subtypes of hepatocellular carcinoma. Cancer Res 2008;68:1451–61.
17. Yamashita T, Budhu A, Forgues M, Wang XW. Activation of hepatic stem cell marker EpCAM by Wnt-β-catenin signaling in hepatocellular carcinoma. Cancer Res 2007;67:10831–9.
18. Yamashita T, Ji J, Budhu A, et al. EpCAM-positive hepatocellular carcinoma cells are tumor-initiating cells with stem/progenitor cell features. Gastroenterology 2009;136:1012–24.
19. Boman BM, Huang E. Human colon cancer stem cells: a new paradigm in gastrointestinal oncology. J Clin Oncol 2008;26:2828–38.
20. Dean M, Fojo T, Bates S. Tumour stem cells and drug resistance. Nat Rev Cancer 2005;5:275–84.
21. Zou GM. Cancer initiating cells or cancer stem cells in the gastrointestinal tract and liver. J Cell Physiol 2008;217:598–604.
22. Hill RP, Perris R. "Destemming" cancer stem cells. J Natl Cancer Inst 2007;99:1435–40.
23. Lee J, Son MJ, Woolard K, et al. Epigenetic-mediated dysfunction of the bone morphogenetic protein pathway inhibits differentiation of glioblastoma-initiating cells. Cancer Cell 2008;13:69–80.
24. Piccirillo SG, Reynolds BA, Zanetti N, et al. Bone morphogenetic proteins inhibit the tumorigenic potential of human brain tumour-initiating cells. Nature 2006;444:761–5.
25. Nasr R, Guillemin MC, Ferhi O, et al. Eradication of acute promyelocytic leukemia-initiating cells through PML-RARA degradation. Nat Med 2008;14:1333–42.
26. Kamiya A, Kinoshita T, Ito Y, et al. Fetal liver development requires a paracrine action of oncostatin M through the gp130 signal transducer. EMBO J 1999;18:2127–36.
27. Kinoshita T, Miyajima A. Cytokine regulation of liver development. Biochim Biophys Acta 2002;1592:303–12.
28. Yamashita T, Honda M, Takatori H, et al. Activation of lipogenic pathway correlates with cell proliferation and poor prognosis in hepatocellular carcinoma. J Hepatol 2009;50:100–10.
29. Lobo NA, Shimono Y, Qian D, Clarke MF. The biology of cancer stem cells. Annu Rev Cell Dev Biol 2007;23:675–99.
30. Heinrich PC, Behrmann I, Haan S, Hermanns HM, Muller-Newen G, Schaper F. Principles of interleukin (IL)-6-type cytokine signalling and its regulation. Biochem J 2003;374:1–20.
31. Deng G, Kakar S, Okudiara K, Choi E, Sleisenger MH, Kim YS. Unique methylation pattern of oncostatin m receptor gene in cancers of colorectum and other digestive organs. Clin Cancer Res 2009; 15:1519–26.
32. Kim MS, Louwagie J, Carvalho B, et al. Promoter DNA methylation of oncostatin m receptor-β as a novel diagnostic and therapeutic marker in colon cancer. PLoS One 2009;4:e6555.
33. Bao S, Wu Q, McLendon RE, et al. Glioma stem cells promote radioresistance by preferential activation of the DNA damage response. Nature 2006;444:756–60.
34. Viale A, De Franco F, Orleth A, et al. Cell-cycle restriction limits DNA damage and maintains self-renewal of leukaemia stem cells. Nature 2009;457:51–6.
35. Gupta PB, Onder TT, Jiang G, et al. Identification of selective inhibitors of cancer stem cells by high-throughput screening. Cell 2009; 138:645–59.
36. Sipkins DA. Rendering the leukemia cell susceptible to attack. N Engl J Med 2009;361:1307–9.
37. Yin C, Lin Y, Zhang X, et al. Differentiation therapy of hepatocellular carcinoma in mice with recombinant adenovirus carrying hepatocyte nuclear factor-4α gene. Hepatology 2008;48:1528–39.

JOURNAL OF VIROLOGY, Sept. 2010, p. 9118–9127
0022-538X/10/$12.00 doi:10.1128/JVI.00402-10

Vol. 84, No. 18

A Disulfide-Bonded Dimer of the Core Protein of Hepatitis C Virus Is Important for Virus-Like Particle Production[▽]†

Yukihiro Kushima,[1,2] Takaji Wakita,[3] and Makoto Hijikata[1,2]*

Department of Viral Oncology, Institute for Virus Research, Kyoto University, Kyoto 606-8507, Japan[1]; Graduate School of Biostudies, Kyoto University, Kyoto 606-8507, Japan[2]; and Department of Virology II, National Institute of Infectious Diseases, Tokyo 162-8640, Japan[3]

Received 24 February 2010/Accepted 20 June 2010

Hepatitis C virus (HCV) core protein forms the nucleocapsid of the HCV particle. Although many functions of core protein have been reported, how the HCV particle is assembled is not well understood. Here we show that the nucleocapsid-like particle of HCV is composed of a disulfide-bonded core protein complex (dbc-complex). We also found that the disulfide-bonded dimer of the core protein (dbd-core) is formed at the endoplasmic reticulum (ER), where the core protein is initially produced and processed. Mutational analysis revealed that the cysteine residue at amino acid position 128 (Cys128) of the core protein, a highly conserved residue among almost all reported isolates, is responsible for dbd-core formation and virus-like particle production but has no effect on the replication of the HCV RNA genome or the several known functions of the core protein, including RNA binding ability and localization to the lipid droplet. The Cys128 mutant core protein showed a dominant negative effect in terms of HCV-like particle production. These results suggest that this disulfide bond is critical for the HCV virion. We also obtained the results that the dbc-complex in the nucleocapsid-like structure was sensitive to proteinase K but not trypsin digestion, suggesting that the capsid is built up of a tightly packed structure of the core protein, with its amino (N)-terminal arginine-rich region being concealed inside.

Hepatitis C virus (HCV) infection is a major cause of chronic hepatitis, liver cirrhosis, and hepatocellular carcinoma, affecting approximately 200 million people worldwide (13, 29, 44). Current treatment strategies, including interferon coupled with ribavirin, are not effective for all patients infected with HCV. An error-prone replication strategy allows HCV to undergo rapid mutational evolution in response to immune pressure and thus evade adaptive immune responses (10). New approaches to HCV therapy include the development of specifically targeted antiviral therapies for hepatitis C (STAT-Cs) which target such HCV proteins as the nonstructural 3/4A (NS3/4A), serine protease, and RNA-dependent RNA polymerase NS5B proteins (3). Despite the potent antiviral activities of some of these approaches, many resistant HCV strains have been reported after treatment with existing STAT-Cs (23, 48, 51). Therefore, identification of new targets that are common to all HCV strains and that are associated with low mutation rates is an area of active research.

HCV has a 9.6-kb, plus-strand RNA genome composed of a 5′ untranslated region (UTR), an open reading frame that encodes a single polyprotein of about 3,000 amino acids, and a 3′ UTR. The polyprotein is processed by host and viral proteases to produce three structural proteins (the core, envelope 1 [E1], and E2 proteins) and seven nonstructural proteins (the p7, NS2, NS3, NS4A, NS4B, NS5A, and NS5B proteins) (14, 16, 17, 22, 49). The HCV core protein is produced cotranslationally via carboxyl (C)-terminal cleavage to generate an immature core protein, 191 amino acids in length, on the endoplasmic reticulum (ER) (16). This protein consists of three predicted domains: the N-terminal hydrophilic domain (D1), the C-terminal hydrophobic domain (D2), and the tail domain (33), which serves as a signal peptide for the E1 protein. D1 includes a number of positively charged amino acids responsible for viral RNA binding (amino acids 1 to 75) (43) and the region involved in multimerization of the core protein via homotypic interactions (amino acids 36 to 91 and 82 to 102) (32, 40) (see Fig. S1 in the supplemental material). Hydrophobic D2 includes the region responsible for core protein association with lipid droplets (LDs; amino acids 125 to 144) (7, 18, 37), which accumulate in response to core protein production (1, 6).

Many functions of the core protein have been reported (13, 38, 50), yet because infectious HCV particles cannot be appropriately produced in currently available experimental systems, HCV particle assembly has not been elucidated to date. A cell culture system that reproduces the complete life cycle of HCV *in vitro* was developed by Wakita et al. using a cloned HCV genome (JFH1) (53). Using this system, the assembly of infectious HCV particles was found to occur near LDs and ER-derived LD-associated membranes (36, 47). Neither the structures nor the functions of the virus proteins involved in virus particle assembly are known, however. To elucidate this point, we have analyzed the biochemical characteristics of the proteins within the fraction containing the HCV particle and found a disulfide-bonded core protein complex (dbc-complex). We revealed that the disulfide-bonded dimer of core protein (dbd-core) was formed by a single cysteine residue at amino

* Corresponding author. Mailing address: Department of Viral Oncology, Institute for Virus Research, Kyoto University, 53 Kawaharacho Shougoin, Kyoto 606-8507, Japan. Phone: 81-75-751-4046. Fax: 81-75-751-3998. E-mail: mhijikat@virus.kyoto-u.ac.jp.

† Supplemental material for this article may be found at http://jvi.asm.org/.

▽ Published ahead of print on 30 June 2010.

acid position 128 on the ER. The roles of the disulfide bond of the core protein in virus-like particle formation are discussed in this paper.

MATERIALS AND METHODS

Cell culture. Cells of the HuH-7 and HuH-7.5 human hepatoma cell lines were grown in Dulbecco's modified Eagle's medium (Nacalai Tesque, Kyoto, Japan) supplemented with 10% fetal bovine serum, 100 U/ml nonessential amino acids (Invitrogen, Carlsbad, CA), and 100 μg/ml each penicillin and streptomycin sulfate (Invitrogen).

Antibodies. The antibodies used for immunoblotting and indirect immunofluorescence analysis were specific for core protein (antibody 32-1), FLAG M2 (Sigma-Aldrich, St. Louis, MO), c-myc (Sigma-Aldrich), NS5A protein (CL1), adipocyte differentiation-related protein (ADRP; StressGen, Victoria, British, Columbia, Canada), calnexin (Calnexin-NT; StressGen), and glyceraldehyde-3-phosphate dehydrogenase (GAPDH; Chemicon, Temecula, CA). Antibodies specific for core protein (antibody 32-1) were a gift from M. Kohara (The Tokyo Metropolitan Institute of Medical Science, Tokyo, Japan). Rabbit polyclonal anti-NS5A protein CL1 antibodies have been described previously (36).

Plasmid construction. All plasmids were generated by inserting PCR-amplified fragments into expression plasmids. The plasmids, primer sequences, templates for the PCRs, and restriction enzyme sites used to construct the plasmids are listed in Table S1 in the supplemental material. Plasmids pJFH1^{E2FL} (encoding the full-length HCV genome with the FLAG epitope in the E2 hypervariable region), pJFH1^{AAA99} (encoding a NS5A mutant of JFH1^{E2FL}, resulting in noninfectious HCV particles), pJFH1$^{PP/AA}$ (encoding a core protein mutant of JFH1^{E2FL}, which allows replication in cells but prevents HCV particle production), and pcDNA3-core^{WT} (an expression plasmid encoding the full-length core protein of JFH1) have been described previously (36). Plasmid pJ6/JFH1, which contains the full-length HCV genome encoding structural proteins from the J6 strain and nonstructural proteins from the JFH1 strain, was kindly provided by Charles M. Rice (The Rockefeller University, New York, NY).

***In vitro* transcription.** RNA for transfection was synthesized as described previously (36). In brief, plasmids carrying the HCV RNA sequence were linearized with XbaI and used as templates for *in vitro* transcription with MEGAscript T7 (Ambion, Austin, TX).

Transfection. Ten micrograms of JFH1^{E2FL}, JFH1^{C128A}, JFH1^{C184A}, JFH1$^{C128/184A}$, JFH1$^{PP/AA}$, or JFH^{AAA99} and J6/JFH1 or J6/JFH1^{AAA99} RNAs were transfected into HuH-7 and HuH-7.5 cells (1.0×10^7 cells) by electroporation (260 V, 0.95 μF) using a Gene Pulser II system (Bio-Rad, Hercules, CA). Core protein expression plasmids were transfected into HuH-7 cells using Lipofectamine LTX (Invitrogen), according to the manufacturer's protocol.

HCV particle precipitation. Culture medium from HCV RNA-transfected cells were concentrated using Amicon Ultra-15 centrifugal filters with Ultracell-100 membranes (Millipore, Billerica, MA) and mixed with sucrose solution in phosphate-buffered saline (PBS) to a final sucrose concentration of 2%. This mixture was ultracentrifuged (100,000 × *g*, 4°C for 2 h), and the HCV particles were obtained as a pellet. The pellet was then suspended in culture medium for infection experiments or PBS for immunoblot analysis.

Indirect immunofluorescence analysis. Indirect immunofluorescence analyses of HCV infection and the cellular localization of the HCV proteins were performed as described previously (36).

Protease protection assay. Concentrated culture medium from JFH1^{E2FL} RNA-transfected HuH-7 cells was fractionated using 20 to 50% sucrose density gradients, and the HCV RNA titer was measured in quantitative reverse transcription-PCRs (RT-PCRs) as described below. Fractions with high HCV RNA titers were collected, and JFH1^{E2FL} particles were obtained as a pellet after ultracentrifugation (100,000 × *g*, 4°C for 2 h). The pellet was suspended in PBS and treated with 10 μg/ml trypsin or 5 μg/ml proteinase K in the presence or absence of 1% Nonidet P-40 (NP-40) at 37°C for 15 min, unless otherwise indicated. The reaction was quenched by the addition of protease inhibitor cocktail (Nacalai Tesque), followed by SDS-PAGE under nonreducing conditions and immunoblotting specific for core protein.

Immunoblot analysis. Samples were subjected to SDS-PAGE in sample buffer (62.5 mM Tris-HCl [pH 7.8], 1% SDS, 10% glycerol) with or without 5% β-mercaptoethanol (β-ME) or 50 mM dithiothreitol (DTT) for reducing and nonreducing conditions, respectively. *N*-Ethylmaleimide (NEM; Nacalai Tesque) was added to the sample buffer to a final concentration of 5 mM for the indicated samples. Proteins were transferred to a polyvinylidene difluoride membrane and blocked in blocking buffer for 1 h at room temperature with gentle agitation. After incubation with primary antibodies overnight at 4°C, the membrane was washed three times for 5 min in washing buffer at room temperature with gentle agitation. The membrane was then incubated with horseradish peroxidase (HRP)-conjugated secondary antibodies for 1 h at room temperature. After three washes in washing buffer, proteins were detected using Western Lightning reagent (PerkinElmer, Waltham, MA) or ECL Advance (GE Healthcare, Buckinghamshire, England) and Kodak MXJB Plus medical X-ray film (Kodak, Rochester, NY) or an LAS-4000 system (Fujifilm, Tokyo, Japan).

Preparation of LDs. LDs were prepared as described previously (36).

Preparation of MMFs. Microsomal membrane fractions (MMFs) were collected as described previously (15) with some modifications. In brief, cells were collected in homogenization buffer (20 mM Tris-HCl [pH 7.8], 250 mM sucrose, and 0.1% ethanol supplemented with protease inhibitor cocktail) and homogenized on ice using 40 strokes of a Dounce homogenizer. The samples were then centrifuged at 1,000 × *g* for 10 min at 4°C. The supernatant was collected in a new tube and centrifuged again at 16,000 × *g* for 20 min at 4°C. The supernatant was further centrifuged at 100,000 × *g* for 1 h at 4°C. The MMF precipitate was homogenized in lysis buffer (1% NP-40, 0.1% SDS, 20 mM Tris-HCl [pH 8.0], 150 mM NaCl, 1 mM EDTA, and 10% glycerol supplemented with protease inhibitor cocktail) using a Dounce homogenizer.

qRT-PCR analysis. Quantitative RT-PCR (qRT-PCR) analysis for determination of the HCV RNA titer was performed as described previously (36).

ELISA specific for core protein. The core protein in culture medium was quantified using an enzyme-linked immunosorbent assay (ELISA; HCV antigen ELISA; Ortho-Clinical Diagnostics, Raritan, NJ), according to the manufacturer's protocol.

RNA-protein binding precipitation assay. Core^{WT} or core^{C128A} was translated *in vitro* from pcDNA3-core^{WT} and pcDNA3-core^{C128A}, respectively, using a TNT-coupled rabbit reticulocyte lysate system (Promega, Madison, WI), according to the manufacturer's protocol. These proteins were incubated with poly(U) agarose (Sigma) in binding buffer (50 mM HEPES (pH 7.4)–100 mM NaCl–0.1% NP-40–20 U RNase inhibitor) at 4°C for 2 h with or without RNase A. After five washes, the resin-bound core proteins were immunoblotted.

RESULTS

The HCV particle contains core protein complex formed by a disulfide bond. To analyze the core protein of the HCV particle, we first subjected the concentrated culture medium of HuH-7 cells transfected with *in vitro*-transcribed JFH1^{E2FL} RNA to ultracentrifugation. After the resulting pellet was resuspended in culture medium, we confirmed the presence of infectious HCV particles on the basis of the infectivity of HuH-7.5 cells (Fig. 1a). The infectious JFH1^{E2FL} particle-containing pellet was separated by SDS-PAGE under nonreducing conditions, and immunoblot analysis showed the presence of a core antibody-reactive protein that was approximately twice the size of the core protein (38 kDa), in addition to the expected 19-kDa core protein (Fig. 1b, lane 1). Because treatment with DTT eliminated the larger core protein antibody-reactive band while the levels of the core protein monomer increased (Fig. 1b, lanes 2 to 6), the larger protein likely represented a dbc-complex. This complex was also found in J6/JFH1-derived particles (see Fig. S2 in the supplemental material), indicating that the complex was not specific for JFH1^{E2FL}.

To determine whether the dbc-complex is a component of the HCV particle, a protease protection assay was performed using RNase-resistant HCV particles fractionated on the basis of their buoyant densities. Concentrated culture medium from HuH-7 cells transfected with *in vitro*-transcribed JFH1^{E2FL} RNA was fractionated using a 20 to 50% sucrose density gradient; and JFH1^{E2FL} particles, which were presumed to contain both infectious and noninfectious particles, were collected from fractions with high HCV RNA titers using ultracentrifugation (Fig. 2a, fractions 8 to 13). The core protein from the collected fractions was analyzed by immunoblotting after SDS-

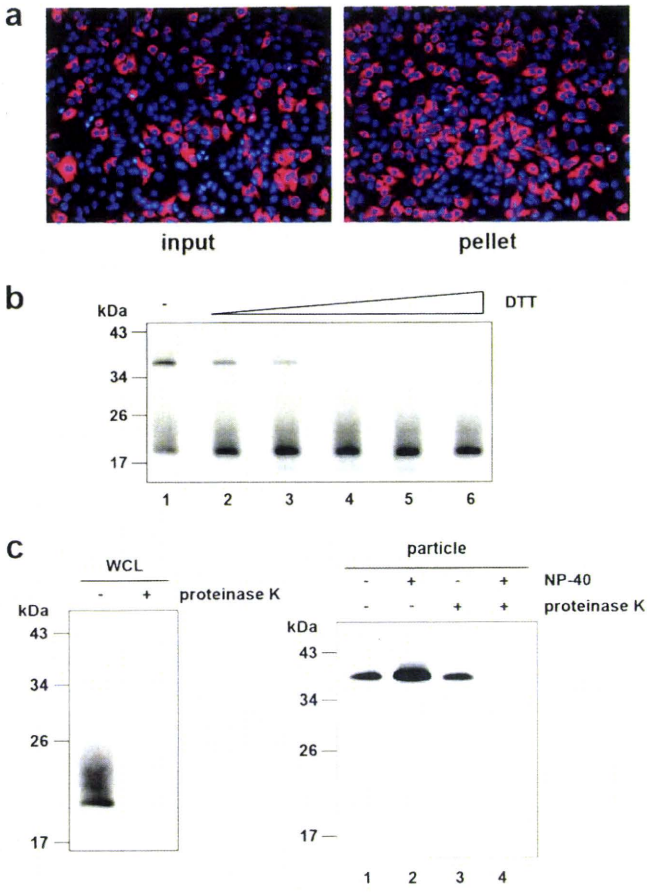

FIG. 1. The HCV-like particle consists of a core complex formed by a disulfide bond. (a) The infectivity of the pellet fraction collected from concentrated culture medium from JFH1^{E2FL} RNA-transfected HuH-7 cells was analyzed as described in Materials and Methods. Input indicates the same volume of concentrated culture medium used to pellet the virus-like particles. (b) Immunoblot analysis of the core protein in pellets containing JFH1^{E2FL} virus particles treated with various levels of DTT (lanes 1, 2, 3, 4, 5, and 6, 0, 1.56, 3.13, 6.25, 12.5, and 25 mM DTT, respectively). (c) Immunoblot analysis of the core protein in JFH1^{E2FL} particles collected from sucrose density gradient fractions with high HCV RNA titers (particle) (Fig. 2a, fractions 8 to 13) and treated with 5 μg/ml proteinase K at 37°C for 15 min in the presence or absence of 1% NP-40 (right panel). As a positive control, WCL prepared from JFH1^{E2FL} RNA-transfected HuH-7 cells in lysis buffer was treated with 5 μg/ml proteinase K at 37°C for 15 min (left panel). Data are representative of three independent experiments.

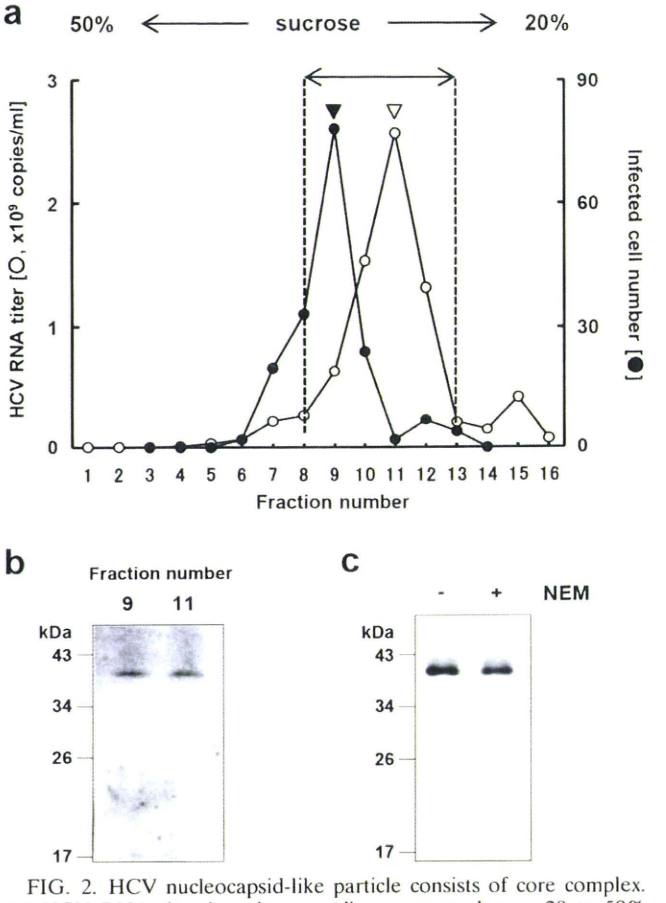

FIG. 2. HCV nucleocapsid-like particle consists of core complex. (a) HCV RNA titer in culture medium separated on a 20 to 50% sucrose density gradient. Concentrated culture medium from JFH1^{E2FL} RNA-transfected HuH-7 cells were treated with RNase and separated on a 20 to 50% sucrose density gradient. Fractions 1 to 16 were obtained from the bottom to the top of the tube, respectively. The HCV RNA titer and infectivity of each fraction were analyzed by real-time qRT-PCR (for fractions 1 to 16) and counting the number of cells infected with HCV-like particle detected by immunofluorescence (for fractions 3 to 14), respectively, as described in Materials and Methods. In brief, each fraction was diluted with 1× PBS and HCV-like particles were collected by ultracentrifugation, and then the pellets were suspended in culture medium and used for infection. (b) HCV-like particle collected from the infectious HCV peak (from panel a, filled arrowhead) and the HCV RNA peak (from panel a, open arrowhead) were collected by ultracentrifugation, subjected to nonreducing SDS-PAGE, and detected by immunoblotting against the core protein. (c) HCV-like particles collected from fractions 8 to 13 (a) were subjected to nonreducing SDS-PAGE in the presence (lane +) or absence (lane −) of 5 mM NEM and analyzed by immunoblotting against the core protein. Data are representative of two (a, infectivity of fractions) or three independent experiments.

PAGE under nonreducing conditions and showed only the dbc-complex (Fig. 1c, right panel).

To examine whether the complex contributes to the infectivity of the particles, we analyzed the dbc-complex in the fractions containing infectious and noninfectious HCV particles (fractions 9 and 11 of Fig. 2a, filled and open arrowheads, respectively). Both the infectious and noninfectious HCV particle-containing fractions contained the dbc-complex (Fig. 2b). To confirm this further, a pellet containing particles of mutant JFH1^{AAA99}—a mutant of JFH1^{E2FL} that primarily produces noninfectious particles (36)—was analyzed in a similar manner. These dbc-complexes were found in pelleted particles of both JFH1^{AAA99} and J6/JFH1^{AAA99}, which was a mutant J6/JFH1 with a similar substitution to JFH1^{AAA99} (see Fig. S2 in the supplemental material). These results indicated that the dbc-complex was present in both the infectious and noninfectious HCV-like particles.

The core protein monomer observed in the pellet samples (Fig. 1b) may be from the secreted core protein or the debris of apoptotic cells, because the core protein is known to be secreted from cells expressing this protein under particular conditions (42) and strain JFH1 is known to cause apoptosis (45). The dbc-complex-specific signals in the HCV particles seem to be increased in the NP-40-treated samples for some

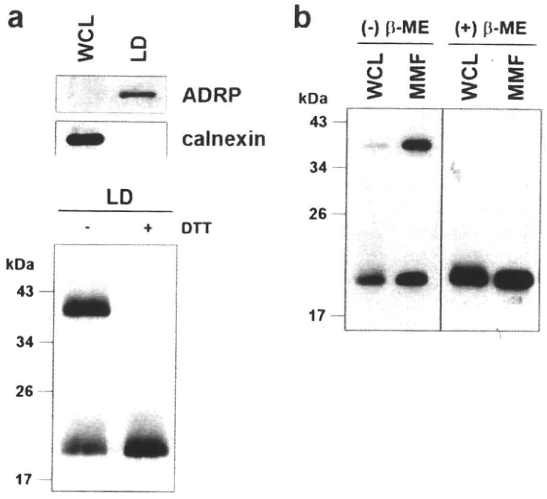

FIG. 3. The core complex is formed at the LD and ER. (a) The LD fraction and WCL were collected from JFH1^{E2FL} RNA-transfected HuH-7 cells on day 5 posttransfection. (upper panel) Immunoblot analysis of the LD marker ADRP and the ER marker calnexin in the LD fraction; (lower panel) immunoblot analysis of the core protein in the LD fraction treated or not treated with 50 mM DTT. (b) Immunoblot analysis of the core protein in the MMF and WCL collected from JFH1^{E2FL}-producing HuH-7 cells on day 5 posttransfection in the presence or absence of 5% β-ME. Data are representative of those from three independent experiments.

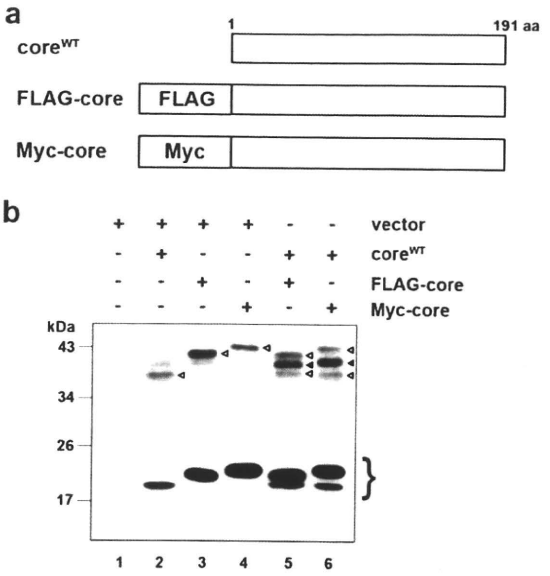

FIG. 4. The core complex consists of a core dimer. (a) Schematic of wild-type, FLAG-tagged (FLAG-core), and Myc-tagged (Myc-core) core proteins. (b) Immunoblot analysis of the core protein in the MMF collected from HuH-7 cells transfected with combinations of pcDNA3 (vector) and/or core expression plasmids (e.g., encoding core^{WT}, FLAG-core, and Myc-core), as indicated. The experiment was performed under nonreducing conditions. The lower bands represent core monomer (marked on the right with a brace). White arrowheads, bands corresponding to dbd-core; black arrowheads, positions of the intermediately sized core complex formed by core^{WT} and the tagged core. Data are representative of those from three independent experiments.

unknown reason (Fig. 1c, lanes 1 and 2). Although the intermolecular disulfide bond is known to be artificially formed in denaturing SDS-PAGE in the absence of reducing agents, the dbc-complex was still observed even in the presence of NEM, which is the alkylating agent for free sulfhydryls, during sample preparation (Fig. 2c), indicating that the dbc-complex was naturally present in the virus-like particles.

The HCV nucleocapsid is covered with lipid membranes and E1 and E2 proteins, making it resistant to proteases. As expected, in the absence of NP-40, the dbc-complex was resistant to proteinase K (Fig. 1c, lane 3), whereas proteinase K was able to digest core protein in whole-cell lysates (WCLs) collected from JFH1^{E2FL}-transfected HuH-7 cells (Fig. 1c, left panel). Disrupting the envelope structure with NP-40 made the dbc-complex susceptible to proteinase K treatment (Fig. 1c, lane 4), indicating that the dbc-complex was indeed a component of the HCV particle.

The dbc-complex forms on the ER. To investigate the subcellular site at which the dbc-complex forms, LDs and MMFs from JFH1^{E2FL} replicating HuH-7 cells were analyzed by immunoblotting. We first analyzed the dbc-complex in LDs, because LDs are involved in infectious HCV particle formation (36, 47). The purity of the LD fraction was determined using immunoblot analysis of calnexin and ADRP, ER and LD marker proteins, respectively (Fig. 3a, upper panel). The core protein was then analyzed in the LD fraction. As shown in Fig. 3a (lower panel), the dbc-complex was observed in the LD fraction from JFH1^{E2FL} RNA-transfected HuH-7 cells. We next analyzed the core protein in the ER-containing MMF, because the core protein is first translated and processed on the ER (16). As shown in Fig. 3b, the dbc-complex was observed in the MMF from JFH1^{E2FL} RNA-transfected HuH-7 cells. These results suggest that the dbc-complex is first formed at the ER. To assess the possibility that dbc-complex-containing HCV particles were also assembled on the ER, the sensitivity of the dbc-complex to protease treatment was analyzed. The dbc-complex in the MMF was susceptible to protease treatment in the absence of NP-40, indicating that the dbc-complex on the ER was not yet part of a HCV particle (data not shown).

dbc-complex is most likely a disulfide-bonded dimer form of the core. In order to examine whether the core protein itself has the potential to form a dbc-complex, we analyzed the dbc-complex formation of the full-length wild-type core protein (core^{WT}) expressed from pcDNA3-core^{WT} (36), the expression plasmid encoding the 191-amino-acid full-length core protein of JFH1 strain. We used this expression plasmid because the core protein from this plasmid was likely to be processed correctly enough to produce infectious HCV particles when it was cotransfected with the RNA of JFH1^{dc3}, which is a core protein deletion mutant of JFH1 (36). As a result, the dbc-complex formation was observed from the MMF of core^{WT}-expressing cells both in the absence and in the presence of NEM (Fig. 4b; lane 2 and data not shown, respectively). We next investigated the effect of the amino acid region of E1 on the production of the dbc-complex, because it has been reported that the efficient processing of core protein is dependent on the presence of some E1 sequence to ensure the insertion of the signal sequence for E1 in the translocon/membrane machinery (34). The dbc-complex was also observed

when the core protein was expressed from pcDNA3-C-E1/25, which encodes the full-length core protein followed by the N-terminal 25-amino-acid sequence of E1 to ensure that the core protein is processed properly (see Fig. S3a in the supplemental material). These data showed that the dbc-complex was formed by expression of the core protein only in the cells.

Next, we examined the structural components of the dbc-complex. Because the dbc-complex was twice the size of the core protein monomer, it was likely dbd-core. So, we investigated whether the core protein molecules with different tags were able to form the dbd-core. We first generated expression plasmids encoding core protein with the N-terminal FLAG and Myc tags (pcDNA3-FLAG-core and pcDNA3-Myc-core, respectively; Fig. 4a). The tagged core proteins were expressed or coexpressed with core^{WT} in HuH-7 cells, and the MMF was analyzed by immunoblotting. The FLAG or Myc tag shifted the positions of the monomer and the complex bands (Fig. 4b, lanes 3 and 4) compared with the position of core^{WT} (Fig. 4b, lane 2). When core^{WT} was coexpressed with FLAG-core or Myc-core, the core protein complex of an intermediate size was observed, in addition to the bands obtained when the constructs were independently expressed (Fig. 4b, lanes 5 and 6, filled arrowheads); the intermediate-sized band disappeared after treatment with β-ME (see Fig. S3b, lanes 11 and 12, filled arrows, in the supplemental material), indicating that core^{WT} and tagged core protein formed a heteromeric disulfide-bonded dimer. These results demonstrated that the dbc-complex on the ER is a dbd-core. Although we tried to detect the hetero- or homodimer consisting of the tagged core protein by using anti-FLAG or anti-Myc antibodies, these dimers were not detected, possibly because of the lower levels of sensitivity and specificity of the antibodies compared to those of the anti-core protein antibody that we used, especially against epitopes in the dbd-core. The results presented above, coupled with the similarities of the molecular sizes and sensitivities to β-ME and DTT, suggested that the dbc-complex in the HCV particle is most likely a dbd-core.

Core protein Cys128 mediates dbd-core formation. Our results showed that core protein from JFH1^{E2FL} forms a disulfide-bonded dimer on the ER. A search for cysteine residues in the JFH1^{E2FL} core protein identified amino acid positions 128 (Cys128) and 184 (Cys184) (see Fig. S1 in the supplemental material). These residues are highly conserved in core proteins from the approximately 2,000 reported HCV strains (HCVdb, http://www.hcvdb.org/, Hepatitis C Virus Database; http://s2as02.genes.nig.ac.jp/). To determine which cysteine residue mediated disulfide bond formation, we generated point mutations in JFH1^{E2FL} that replaced Cys128 and/or Cys184 with alanine (Ala) (C128A, C184A, and C128/184A in JFH1^{C128A}, JFH1^{C184A}, and JFH1$^{C128/184A}$, respectively; Fig. 5a). As shown in Fig. 5b, the core proteins from JFH1^{C128A} and JFH1$^{C128/184A}$ failed to form a dbd-core under nonreducing condition, whereas the core protein from JFH1^{C184A} formed the dimer, indicating that Cys128 was the residue responsible. Similar results were observed when Cys was replaced by serine (Ser) instead of Ala (see Fig. S5c in the supplemental material). Recently, Majeau et al. reported that the core protein of the J6/JFH1 strain with Cys128 replacements by Ala or Ser were unstable in both *Pichia pastoris* and human hepatoma cell line HuH-7.5 (31), although we did not detect any noticeable degradation of the mutant core proteins of strain JFH1 (Fig. 5b; see also Fig. S5c in the supplemental material). This difference may have resulted from the difference in sample preparation methods, as we used the full-length genome of JFH1^{E2FL} strain bearing the strain JFH1 core protein and HuH-7 cells instead of a core protein-expressing plasmid for the J6 strain and HuH-7.5 cells.

To exclude the possibility that mutation of Cys128 inhibited dbd-core formation by creating a conformational change, T127A and G129A core protein mutants (JFH1^{T127A} and JHF1^{G129A}, respectively) were created and examined for their effects on dbd-core formation and infectious virus particle production. These mutants formed dbd-core, and infectious HCV particles were detected in the culture medium (see Fig. S4a to c in the supplemental material), supporting an essential role for Cys128 in dbd-core and particle formation.

dbd-core contributes to HCV particle production. To examine the functional roles of dbd-core, infectious HCV particle production, HCV replication efficiency, colocalization of the core protein and LDs, and RNA binding of mutant and wild-type (JFH1^{E2FL}) core protein were evaluated. Culture medium from HuH-7 cells transfected with JFH1^{C128A} or JFH1$^{C128/184A}$ RNA contained significantly fewer infectious HCV particles compared with the numbers obtained with JFH1^{E2FL} or JFH1^{C184A} RNA (Fig. 5c). We also found significant decreases in the levels of HCV RNA and core protein in the culture medium of HuH-7 cells transfected with JFH1^{C128A} or JFH1$^{C128/184A}$ RNA (Fig. 5d and e). Similar results were observed with J6/JFH1 C128A or the C128/184A mutant strain (data not shown). To investigate whether these results were due to suppressed HCV replication, the HCV RNA and protein levels in cells transfected with mutant RNA were analyzed using qRT-PCR and immunoblot analyses, respectively. Compared with the results obtained with JFH1^{E2FL}, no significant changes in the cellular HCV RNA titer at days 1, 3, and 5 posttransfection or in the expression of HCV nonstructural protein NS5A were observed (Fig. 6a and b). This indicated that substitution of Cys128 did not significantly affect HCV RNA genome replication or viral protein production, demonstrating that the dbd-core functions during HCV particle production rather than HCV genome replication. Similar results were observed using RNA of JFH1 mutant strain JFH1^{C128S}, in which the cysteine at position 128 was replaced by Ser instead of Ala (see Fig. S5a, b, and d in the supplemental material).

The subcellular localizations of the core protein and NS5A protein in HuH-7 cells transfected with HCV RNA were investigated using indirect immunofluorescence and confocal microscopy, because recruiting HCV proteins to LDs is an important step in infectious HCV particle production (36, 47) and core trafficking to LDs is dependent on signal peptide peptidase (SPP)-mediated cleavage of the tail region (34, 41). JFH1^{C128A} mutant core protein and NS5A protein were efficiently trafficked to LDs, as was observed with wild-type JHF1^{E2FL} (Fig. 6c), suggesting that SPP cleavage and core protein maturation were not affected by the C128A mutation. Similar results were obtained with the core proteins derived from JFH1^{C184A} and JFH1$^{C128/184A}$ (see Fig. S6 in the supplemental material) and also Ser mutant JFH1^{C128S} (see Fig. 5e in the supplemental material).

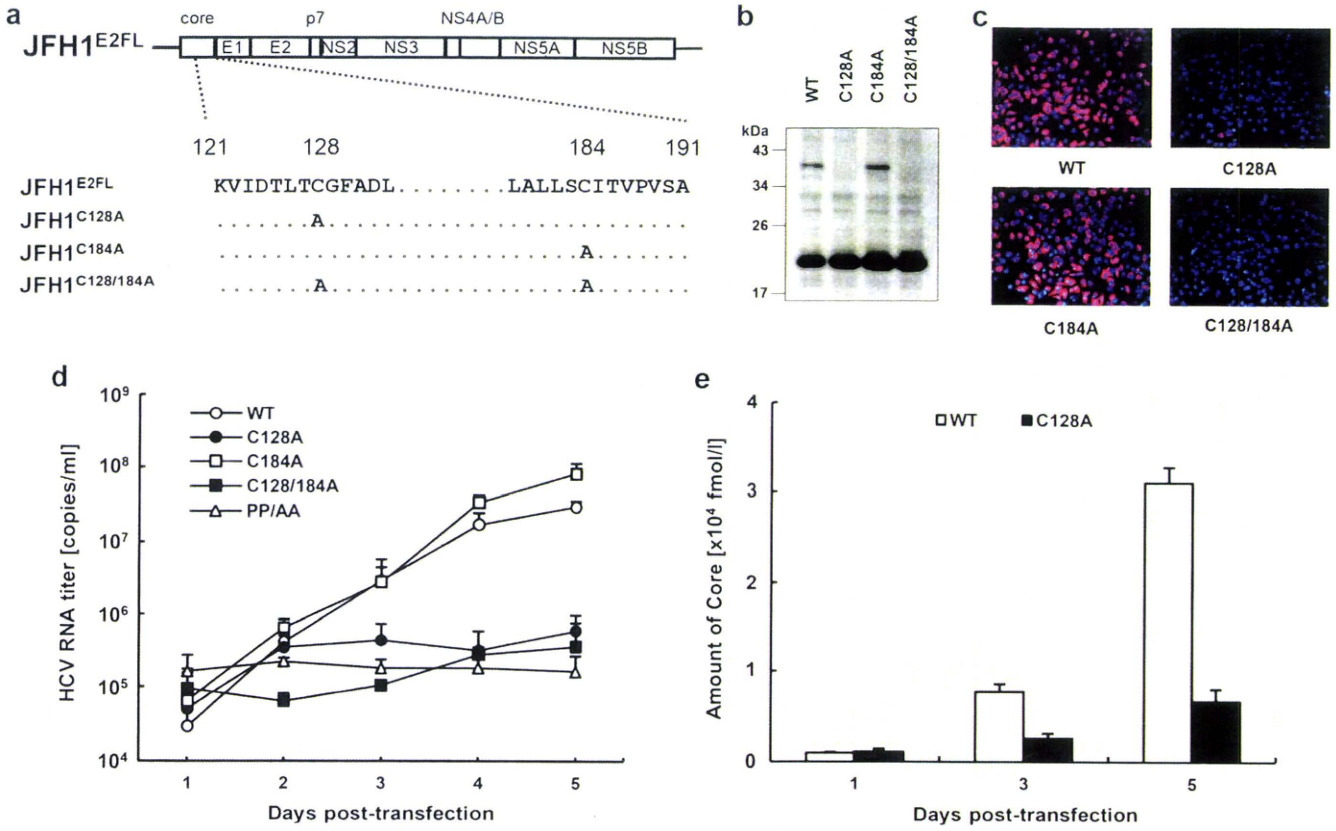

FIG. 5. The core dimer is formed via a bond between cysteine residues at amino acid position 128. (a) Site-directed mutagenesis of JFH1^{E2FL}. (b) Immunoblot analysis of the core protein in MMFs collected from HuH-7 cells under nonreducing conditions 3 days post-transfection with JFH1^{E2FL} (WT), JFH1^{C128A} (C128A), JFH1^{C184A} (C184A), or JFH1$^{C128/184A}$ (C128/184A) RNA. (c) Infectivity of culture medium collected and concentrated on day 5 posttransfection from HuH-7 cells transfected with WT, C128A, C184A, or C128/184A RNA. (d) Real-time qRT-PCR analysis of HCV RNA titers in culture medium collected at the indicated time points from HuH-7 cells transfected with WT, C128A, C184A, C128/184A, or PP/AA (JFH1$^{PP/AA}$) RNA. (e) ELISAs of core protein levels in culture medium collected at the indicated time points from HuH-7 cells transfected with WT or C128A RNA. Data are representative of those from three independent experiments (b and c) or are the means ± standard deviations from three independent experiments (d and e).

Because HCV core protein can bind to RNA, including the HCV genome, during viral particle assembly (43), we analyzed RNA binding by the core protein using *in vitro*-translated core^{C128A}, core^{WT}, and poly(U) agarose resin. Core^{C128A} and core^{WT} bound similarly to the poly(U) resin (Fig. 6d).

dbd-core is important for HCV particle assembly. The mutational analysis of the core protein indicated that core^{C128A} and core^{WT} similarly localize to LDs, recruit NS proteins to the LD, and bind to RNA. Moreover, this mutation did not markedly affect HCV genome replication. How does core^{C128A} affect the production of HCV particles? An important function of the core protein is multimerization, which is followed by capsid construction and packaging of the RNA genome in the viral particles. We therefore determined whether core^{C128A} had a dominant negative effect on virus-like particle production. Wild-type JFH1^{E2FL} RNA and different amounts of JFH1^{C128A} RNA were cotransfected into HuH-7 cells, and the HCV RNA titer and infectivity of the virus-like particles in the culture medium were analyzed. As expected, the HCV RNA titer in the cells increased with higher levels of transfected RNA (see Fig. S7a in the supplemental material). In contrast, the HCV RNA titer and infectivity in the culture medium decreased in a JFH1^{C128A} RNA dose-dependent manner when this mutant RNA was cotransfected with wild-type RNA (Fig. 7a, b). This suppressive effect was not observed when either wild-type RNA or core deletion mutant JFH1^{dc3} RNA was used instead of mutant RNA in a similar experiment (see Fig. S7b to e in the supplemental material), indicating that higher levels of HCV RNA alone did not inhibit HCV particle production. Thus, core^{C128A} had a dominant negative effect on HCV particle production. Together, these results suggest that dbd-core is involved in the assembly of HCV particles.

The nucleocapsid-like particle of HCV was resistant to trypsin treatment. To further investigate the structure of the HCV nucleocapsid-like particle most likely formed by dbd-core, we examined the sensitivity of the particle to trypsin, which cleaves polypeptides at the C-terminal end of basic residues. Whereas trypsin digested the core protein in the whole-cell lysates (Fig. 8a, left panel), dbd-core from buoyant density-fractionated JFH1^{E2FL} particles was resistant to digestion, despite NP-40 treatment (Fig. 8a, right panel), although it was sensitive to proteinase K, which has a broad specificity (Fig. 1c). The N-terminal hydrophilic domain of the core protein (from residues 6 to 121) contains a number of trypsin cleavage sites (25 sites

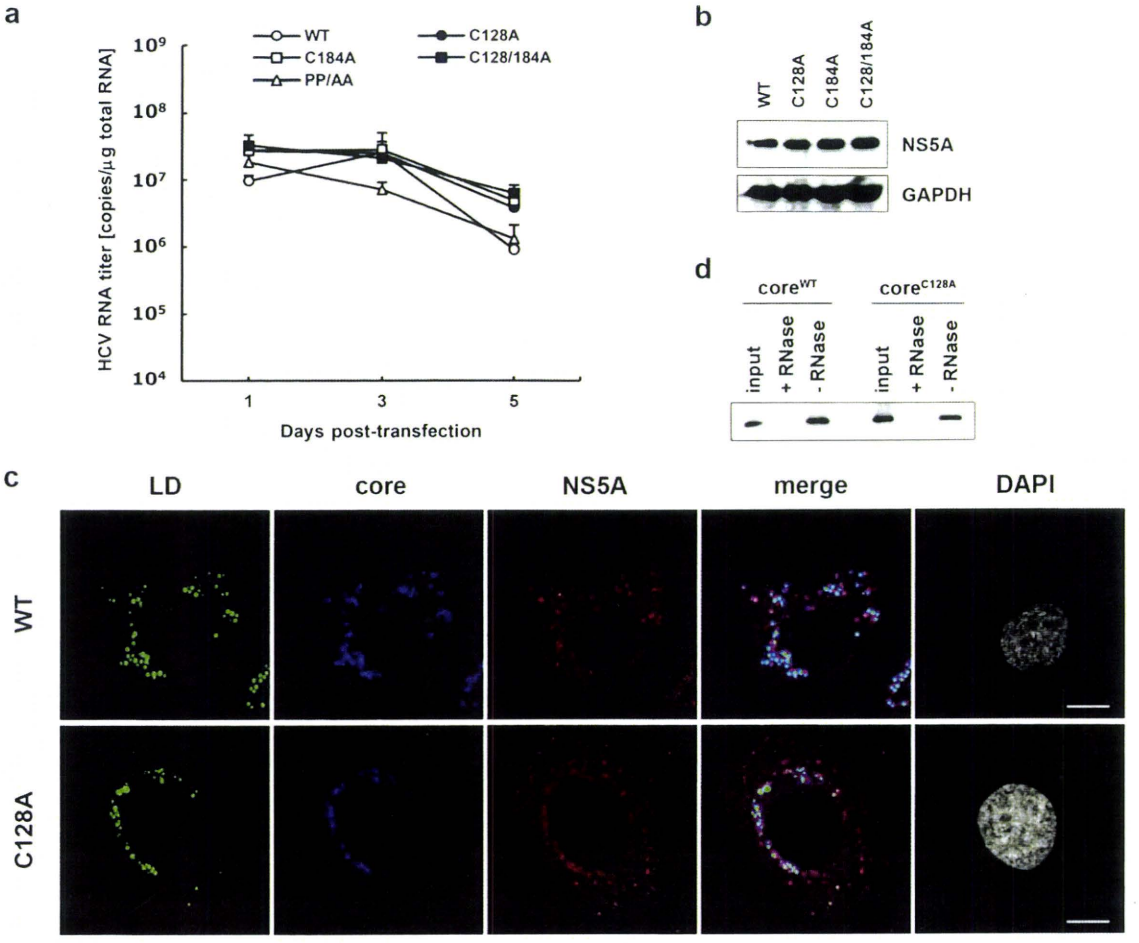

FIG. 6. Site-directed mutagenesis has no effect on HCV replication. (a) Real-time qRT-PCR analysis of the HCV RNA titer using total cellular RNA collected at the indicated time points from cells transfected with JFH1^{E2FL} (WT), JFH1^{C128A} (C128A), JFH1^{C184A} (C184A), JFH1$^{C128/184A}$ (C128/184A), or JFH1$^{PP/AA}$ (PP/AA) RNA. (b) Immunoblot analysis of NS5A protein and GAPDH in whole-cell lysate collected from cells transfected with WT, C128A, C184A, or C128/184A RNA at day 3 posttransfection. (c) Confocal microscopy of the subcellular localization of the LD (green), core (blue), NS5A protein (red), and nucleus (4′,6-diamidino-2-phenylindole [DAPI]) (gray) in WT and C128A replicating cells on day 3 posttransfection. Bars, 10 μm. (d) An RNA-protein binding precipitation assay was performed with *in vitro*-translated core^{WT} and core^{C128A} using poly(U) agarose as the resin. +RNase and −RNase, samples with and without RNase treatment, respectively, as described in Materials and Methods. Input indicates that 1/40 of the amount of translated product was used in this assay. Data represent the means ± standard deviations from three independent experiments (a) or are representative of those from three independent experiments (b to d).

in strain JHF1) (see Fig. S1 in the supplemental material), suggesting that the N-terminal domain faces inward and/or that the conformation prevents protease access. To address this idea, buoyant density-fractionated JFH1^{E2FL} particles were treated with trypsin under stricter conditions in the presence of NP-40. Cleavage of dbd-core by various levels of trypsin correlated with the appearance of a shorter molecule (Fig. 8b, white arrowhead). The shorter molecule was presumed to be partially digested dbd-core with an intact N-terminal region because it was recognized by anti-core protein antibodies, which bind to an epitope located from amino acids 20 to 40 of the core protein (M. Kohara, The Tokyo Metropolitan Institute of Medical Science, personal communication). These results suggest that dbd-core is assembled into the nucleocapsid-like particle such that most of the N-terminal domain is inside.

DISCUSSION

In the present study, we have shown that the nucleocapsid-like particle of HCV most likely contains a dimer of core protein that is stabilized by a disulfide bond. Mutational analysis revealed that Cys128 forms a disulfide bond between core monomers. Several reports have shown that disulfide bonds in the capsid proteins of some viruses are involved in virus particle assembly and stabilization of the viral capsid structure (4, 21, 27, 28, 57); these viruses are characterized by icosahedral nucleocapsids. Because, like these viruses, the HCV virion is spherical (2, 20), it has been suggested that HCV may contain a nucleocapsid with a similar structure (20). We found the dbc-complex, which is most likely to be the dbd-core in JFH1^{E2FL} virus-like particles (Fig. 1c and 8a). The dbd-core in the capsid structure was digested by proteinase K but not

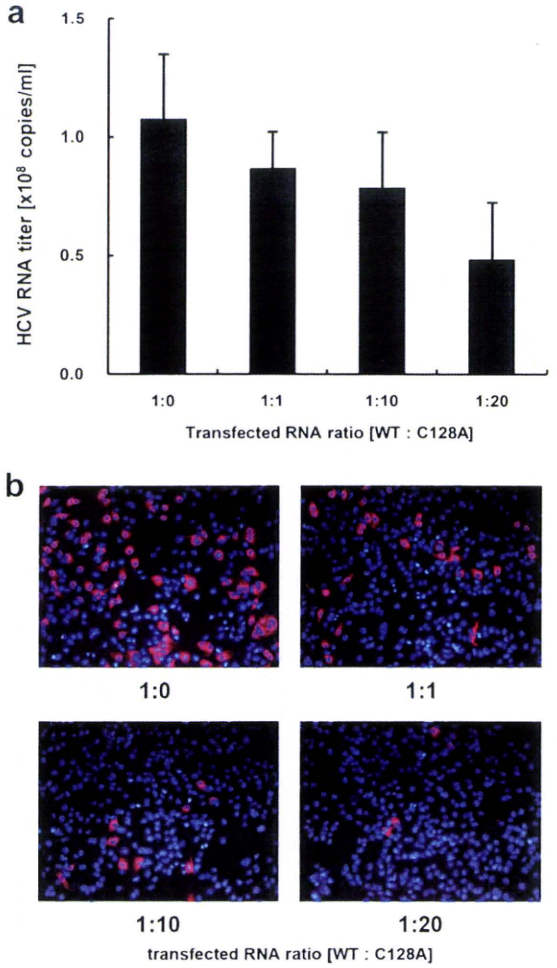

FIG. 7. JFH1^{C128A} core inhibits JFH1^{E2FL} particle assembly. A competitive inhibitory assay was performed with JFH1^{E2FL} (WT) and JFH1^{C128A} (C128A). (a) Real-time qRT-PCR analysis of the HCV RNA titer in HuH-7 cell culture medium 3 days after the cells were transfected with the indicated ratio of WT and C128A RNA. (b) The infectivity of culture medium collected from HuH-7 cells that had been transfected with the indicated ratio of WT and C128A RNA was analyzed as described in Materials and Methods. Data represent the means ± standard deviations from three independent experiments (a) or are representative of those from three independent experiments (b).

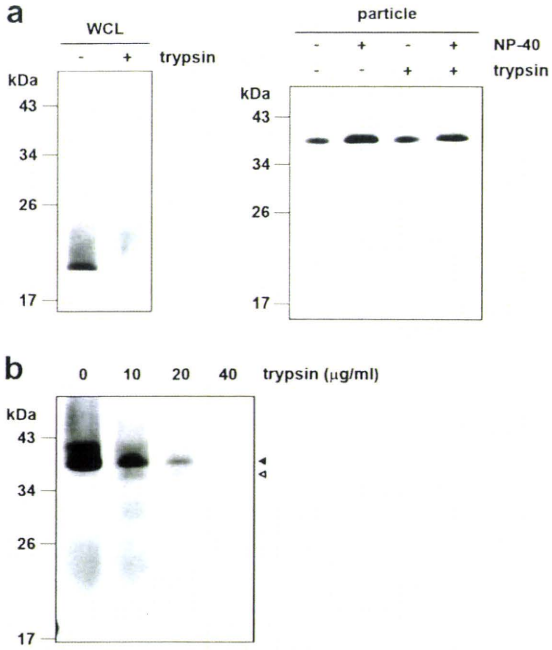

FIG. 8. The nucleocapsid-like particle of JFH1^{E2FL} is assembled with the C-terminal region of the core protein on the outer surface. (a) Immunoblot analysis of the core protein in JFH1^{E2FL} particles collected from sucrose density gradient fractions with high HCV RNA titers (particle) (Fig. 2a, fractions 8 to 13). The fractions were treated with 10 μg/ml trypsin at 37°C for 15 min in the presence or absence of 1% NP-40 (right panel). As a positive control, WCL prepared from JFH1^{E2FL} RNA-transfected HuH-7 cells in lysis buffer was treated with 10 μg/ml trypsin at 37°C for 15 min (left panel). (b) Immunoblot analysis of the core protein in JFH1^{E2FL} particles collected from sucrose density gradient fractions with high HCV RNA titers (Fig. 2a, fractions 8 to 13). The fractions were treated with the indicated concentrations of trypsin at 37°C for 10 min in the presence of 1% NP-40. Open and filled arrows indicate the positions of dbd-core and the trypsin-digested fragment, respectively. Data are representative of those from three independent experiments.

trypsin in the presence of NP-40 (Fig. 1c and 8a, lane 4). The resistance to trypsin suggested a tight conformation for dbd-core in the capsid and no exposed trypsin cleavage sites. The truncated form of dbd-core that was observed under certain trypsin treatment conditions likely resulted from cleavage in the C-terminal portion of the protein (e.g., arginine residues at positions 149 and 156) (see Fig. S1 in the supplemental material), although it is possible that the truncation of dbd-core was due to nonspecific cleavage by trypsin. These results imply that dbd-core is configured such that the N- and C-terminal ends are located at the inner and outer surfaces of the capsid, respectively. Because the N-terminal region of the core protein includes the RNA binding domain (43), the HCV RNA genome likely interacts with the core protein as it is packed in the nucleocapsid. On the other hand, the C-terminal hydrophobic domain probably faces the lipid membranes to form the envelope structure. Only part of the N-terminal hydrophilic region of the core protein has been structurally examined using X-ray crystal structural analysis (35) and structural bioinformatics and nuclear magnetic resonance analysis (11). Although the C-terminal half of the core protein has been structurally investigated by the use of bioinformatics (8), the three-dimensional structure containing the Cys128 residue is unknown. Thus, determination of the structure of the core protein in the nucleocapsid containing the Cys128 residue should be required for understanding the whole structure of this protein in the virus particles.

Because cotransfection of JFH1^{C128A} RNA with wild-type JFH1^{E2FL} RNA inhibited particle production in a mutant RNA dose-dependent manner (Fig. 7a and b), the C128A core variant clearly inhibited HCV particle formation by wild-type core protein. Cys128 was also previously reported to be a residue included in the region important for the production of infectious HCV (39). This residue is located near the N-terminal end of the hydrophobic region of the core (amino acids 122 to 177) and belongs to the hydrophilic side of an amphipathic helix expected to interact in the plane of the membrane interface (7). Therefore, it is possible to think that dbd-core

formation via Cys128 can stabilize the interaction between the core protein and the membranes. The N-terminal half of the core protein (amino acids 1 to 124) reportedly assembles into nucleocapsid-like particles in the presence of the 5′ UTR from HCV RNA (24), suggesting that some nucleocapsid-like particles may assemble via only homotypic interactions from the core protein. In addition to weak homotypic interactions, the HCV core protein forms a disulfide bond to stabilize the capsid structure, thus making dbd-core indispensable in the stable virus-like particle. We observed that culture medium from JFH1^{C128A}- or JFH1^{C128S}-transfected cells included slight infectivity (Fig. 5c; see also Fig. S5d in the supplemental material). This made us speculate that this mutant may produce some infective particle-like structure formed by a homotypic interaction of the core. Such a slight infectivity may have reflected the optimized *in vitro* culture conditions compared with the *in vivo* conditions, allowing relatively unstable virus particles to survive.

A nucleocapsid must be resistant to environmental degradation yet still be able to disassemble after infection. Disulfide bonds could help with this process by switching between a stable and unstable virus capsid on the basis of different intracellular and extracellular oxidation conditions (12, 30). During the virus life cycle, the disulfide bond strengthens the viral capsid structure and protects the viral genome from oxidative conditions and cellular nucleases when virus particles are formed. Upon infection, the disulfide bond may be cleaved under cytoplasmic reducing conditions, thereby releasing the viral genome into the cell for replication. HCV may utilize the core protein disulfide bond in this way as HCV enters the host cell via clathrin-mediated endocytosis (5) into a low-pH, endosomal compartment (25, 52); this is presumably followed by endosomal membrane fusion and release of the viral capsid into the cytoplasm (38).

Treatment of HCV infection with pegylated interferon in combination with ribavirin is not effective for all patients. Recently, drugs targeting viral proteins NS3/4A and NS5B have been examined in clinical trials. Although these drugs are relatively specific, resulting in fewer side effects and potent antiviral activity, monotherapy can be complicated by rapidly emerging resistant variants carrying mutations that reduce drug efficacy, perhaps due to conformational changes in the target (23, 48, 51). Therefore, viral proteins that are highly conserved among strains and those characterized by low mutation rates may be better targets for drug development. Because the core protein is the most conserved HCV protein and Cys128 is conserved among almost all HCV strains examined, drugs that interact with Cys128 and/or the region around or near this residue will likely show broad-spectrum efficacy to block stable infectious particle formation. Structural analysis of dbd-core should aid with the development of new STAT-Cs that target Cys128 by direct interaction with the sulfide group and/or region around this residue. Until now and still, the mechanism of disulfide bond formation of the core protein on the ER is unknown. Dimerization of the capsid protein by disulfide bond has been reported in some enveloped viruses (9, 19, 54, 56), although some were shown not to be important for virus particle formation (26, 55). Unlike vaccinia virus (46), no redox system of its own has been reported for these viruses. Therefore, further investigations addressing the mechanisms underlying dbd-core formation on the ER may reveal a new mechanism for disulfide bond formation of viral proteins in infected cells.

ACKNOWLEDGMENTS

This work was supported by grants-in-aid from the Ministry of Health, Labor, and Welfare of Japan and by grants-in-aid from the Japan Health Sciences Foundation.

REFERENCES

1. **Abid, K., V. Pazienza, A. de Gottardi, L. Rubbia-Brandt, B. Conne, P. Pugnale, C. Rossi, A. Mangia, and F. Negro.** 2005. An in vitro model of hepatitis C virus genotype 3a-associated triglycerides accumulation. J. Hepatol. **42**:744–751.
2. **Aly, H. H., Y. Qi, K. Atsuzawa, N. Usuda, Y. Takada, M. Mizokami, K. Shimotohno, and M. Hijikata.** 2009. Strain-dependent viral dynamics and virus-cell interactions in a novel in vitro system supporting the life cycle of blood-borne hepatitis C virus. Hepatology **50**:689–696.
3. **Asselah, T., Y. Benhamou, and P. Marcellin.** 2009. Protease and polymerase inhibitors for the treatment of hepatitis C. Liver Int. **29**(Suppl. 1):57–67.
4. **Baron, M. D., and K. Forsell.** 1991. Oligomerization of the structural proteins of rubella virus. Virology **185**:811–819.
5. **Blanchard, E., S. Belouzard, L. Goueslain, T. Wakita, J. Dubuisson, C. Wychowski, and Y. Rouille.** 2006. Hepatitis C virus entry depends on clathrin-mediated endocytosis. J. Virol. **80**:6964–6972.
6. **Boulant, S., M. W. Douglas, L. Moody, A. Budkowska, P. Targett-Adams, and J. McLauchlan.** 2008. Hepatitis C virus core protein induces lipid droplet redistribution in a microtubule- and dynein-dependent manner. Traffic **9**:1268–1282.
7. **Boulant, S., R. Montserret, R. G. Hope, M. Ratinier, P. Targett-Adams, J. P. Lavergne, F. Penin, and J. McLauchlan.** 2006. Structural determinants that target the hepatitis C virus core protein to lipid droplets. J. Biol. Chem. **281**:22236–22247.
8. **Boulant, S., C. Vanbelle, C. Ebel, F. Penin, and J. P. Lavergne.** 2005. Hepatitis C virus core protein is a dimeric alpha-helical protein exhibiting membrane protein features. J. Virol. **79**:11353–11365.
9. **Cornillez-Ty, C. T., and D. W. Lazinski.** 2003. Determination of the multimerization state of the hepatitis delta virus antigens in vivo. J. Virol. **77**:10314–10326.
10. **Dustin, L. B., and C. M. Rice.** 2007. Flying under the radar: the immunobiology of hepatitis C. Annu. Rev. Immunol. **25**:71–99.
11. **Duvignaud, J. B., C. Savard, R. Fromentin, N. Majeau, D. Leclerc, and S. M. Gagne.** 2009. Structure and dynamics of the N-terminal half of hepatitis C virus core protein: an intrinsically unstructured protein. Biochem. Biophys. Res. Commun. **378**:27–31.
12. **Freedman, R. B., B. E. Brockway, and N. Lambert.** 1984. Protein disulphide-isomerase and the formation of native disulphide bonds. Biochem. Soc. Trans. **12**:929–932.
13. **Giannini, C., and C. Brechot.** 2003. Hepatitis C virus biology. Cell Death Differ. **10**(Suppl. 1):S27–S38.
14. **Grakoui, A., C. Wychowski, C. Lin, S. M. Feinstone, and C. M. Rice.** 1993. Expression and identification of hepatitis C virus polyprotein cleavage products. J. Virol. **67**:1385–1395.
15. **Higashi, Y., H. Itabe, H. Fukase, M. Mori, Y. Fujimoto, R. Sato, T. Imanaka, and T. Takano.** 2002. Distribution of microsomal triglyceride transfer protein within sub-endoplasmic reticulum regions in human hepatoma cells. Biochim. Biophys. Acta **1581**:127–136.
16. **Hijikata, M., N. Kato, Y. Ootsuyama, M. Nakagawa, and K. Shimotohno.** 1991. Gene mapping of the putative structural region of the hepatitis C virus genome by in vitro processing analysis. Proc. Natl. Acad. Sci. U. S. A. **88**:5547–5551.
17. **Hijikata, M., H. Mizushima, Y. Tanji, Y. Komoda, Y. Hirowatari, T. Akagi, N. Kato, K. Kimura, and K. Shimotohno.** 1993. Proteolytic processing and membrane association of putative nonstructural proteins of hepatitis C virus. Proc. Natl. Acad. Sci. U. S. A. **90**:10773–10777.
18. **Hope, R. G., and J. McLauchlan.** 2000. Sequence motifs required for lipid droplet association and protein stability are unique to the hepatitis C virus core protein. J. Gen. Virol. **81**:1913–1925.
19. **Hu, H. M., K. N. Shih, and S. J. Lo.** 1996. Disulfide bond formation of the in vitro-translated large antigen of hepatitis D virus. J. Virol. Methods **60**:39–46.
20. **Ishida, S., M. Kaito, M. Kohara, K. Tsukiyama-Kohora, N. Fujita, J. Ikoma, Y. Adachi, and S. Watanabe.** 2001. Hepatitis C virus core particle detected by immunoelectron microscopy and optical rotation technique. Hepatol. Res. **20**:335–347.
21. **Jeng, K. S., C. P. Hu, and C. M. Chang.** 1991. Differential formation of disulfide linkages in the core antigen of extracellular and intracellular hepatitis B virus core particles. J. Virol. **65**:3924–3927.
22. **Kato, N., M. Hijikata, Y. Ootsuyama, M. Nakagawa, S. Ohkoshi, T. Sug-**

imura, and K. Shimotohno. 1990. Molecular cloning of the human hepatitis C virus genome from Japanese patients with non-A, non-B hepatitis. Proc. Natl. Acad. Sci. U. S. A. 87:9524–9528.
23. Kieffer, T. L., A. D. Kwong, and G. R. Picchio. 2010. Viral resistance to specifically targeted antiviral therapies for hepatitis C (STAT-Cs). J. Antimicrob. Chemother. 65:202–212.
24. Kim, M., Y. Ha, and H. J. Park. 2006. Structural requirements for assembly and homotypic interactions of the hepatitis C virus core protein. Virus Res. 122:137–143.
25. Koutsoudakis, G., A. Kaul, E. Steinmann, S. Kallis, V. Lohmann, T. Pietschmann, and R. Bartenschlager. 2006. Characterization of the early steps of hepatitis C virus infection by using luciferase reporter viruses. J. Virol. 80:5308–5320.
26. Lee, J. Y., D. Hwang, and S. Gillam. 1996. Dimerization of rubella virus capsid protein is not required for virus particle formation. Virology 216:223–227.
27. Li, M., P. Beard, P. A. Estes, M. K. Lyon, and R. L. Garcea. 1998. Intercapsomeric disulfide bonds in papillomavirus assembly and disassembly. J. Virol. 72:2160–2167.
28. Li, P. P., A. Nakanishi, S. W. Clark, and H. Kasamatsu. 2002. Formation of transitory intrachain and interchain disulfide bonds accompanies the folding and oligomerization of simian virus 40 Vp1 in the cytoplasm. Proc. Natl. Acad. Sci. U. S. A. 99:1353–1358.
29. Liang, T. J., L. J. Jeffers, K. R. Reddy, M. De Medina, I. T. Parker, H. Cheinquer, V. Idrovo, A. Rabassa, and E. R. Schiff. 1993. Viral pathogenesis of hepatocellular carcinoma in the United States. Hepatology 18:1326–1333.
30. Liljas, L. 1999. Virus assembly. Curr. Opin. Struct. Biol. 9:129–134.
31. Majeau, N., R. Fromentin, C. Savard, M. Duval, M. J. Tremblay, and D. Leclerc. 2009. Palmitoylation of hepatitis C virus core protein is important for virion production. J. Biol. Chem. 284:33915–33925.
32. Matsumoto, M., S. B. Hwang, K. S. Jeng, N. Zhu, and M. M. Lai. 1996. Homotypic interaction and multimerization of hepatitis C virus core protein. Virology 218:43–51.
33. McLauchlan, J. 2000. Properties of the hepatitis C virus core protein: a structural protein that modulates cellular processes. J. Viral Hepat. 7:2–14.
34. McLauchlan, J., M. K. Lemberg, G. Hope, and B. Martoglio. 2002. Intramembrane proteolysis promotes trafficking of hepatitis C virus core protein to lipid droplets. EMBO J. 21:3980–3988.
35. Menez, R., M. Bossus, B. H. Muller, G. Sibai, P. Dalbon, F. Ducancel, C. Jolivet-Reynaud, and E. A. Stura. 2003. Crystal structure of a hydrophobic immunodominant antigenic site on hepatitis C virus core protein complexed to monoclonal antibody 19D9D6. J. Immunol. 170:1917–1924.
36. Miyanari, Y., K. Atsuzawa, N. Usuda, K. Watashi, T. Hishiki, M. Zayas, R. Bartenschlager, T. Wakita, M. Hijikata, and K. Shimotohno. 2007. The lipid droplet is an important organelle for hepatitis C virus production. Nat. Cell Biol. 9:1089–1097.
37. Moradpour, D., C. Englert, T. Wakita, and J. R. Wands. 1996. Characterization of cell lines allowing tightly regulated expression of hepatitis C virus core protein. Virology 222:51–63.
38. Moradpour, D., F. Penin, and C. M. Rice. 2007. Replication of hepatitis C virus. Nat. Rev. Microbiol. 5:453–463.
39. Murray, C. L., C. T. Jones, J. Tassello, and C. M. Rice. 2007. Alanine scanning of the hepatitis C virus core protein reveals numerous residues essential for production of infectious virus. J. Virol. 81:10220–10231.
40. Nolandt, O., V. Kern, H. Muller, E. Pfaff, L. Theilmann, R. Welker, and H. G. Krausslich. 1997. Analysis of hepatitis C virus core protein interaction domains. J. Gen. Virol. 78(Pt 6):1331–1340.
41. Okamoto, K., Y. Mori, Y. Komoda, T. Okamoto, M. Okochi, M. Takeda, T. Suzuki, K. Moriishi, and Y. Matsuura. 2008. Intramembrane processing by signal peptide peptidase regulates the membrane localization of hepatitis C virus core protein and viral propagation. J. Virol. 82:8349–8361.
42. Sabile, A., G. Perlemuter, F. Bono, K. Kohara, F. Demaugre, M. Kohara, Y. Matsuura, T. Miyamura, C. Brechot, and G. Barba. 1999. Hepatitis C virus core protein binds to apolipoprotein AII and its secretion is modulated by fibrates. Hepatology 30:1064–1076.
43. Santolini, E., G. Migliaccio, and N. La Monica. 1994. Biosynthesis and biochemical properties of the hepatitis C virus core protein. J. Virol. 68:3631–3641.
44. Seeff, L. B., and J. H. Hoofnagle. 2003. Appendix: The National Institutes of Health Consensus Development Conference Management of Hepatitis C 2002. Clin. Liver Dis. 7:261–287.
45. Sekine-Osajima, Y., N. Sakamoto, K. Mishima, M. Nakagawa, Y. Itsui, M. Tasaka, Y. Nishimura-Sakurai, C. H. Chen, T. Kanai, K. Tsuchiya, T. Wakita, N. Enomoto, and M. Watanabe. 2008. Development of plaque assays for hepatitis C virus-JFH1 strain and isolation of mutants with enhanced cytopathogenicity and replication capacity. Virology 371:71–85.
46. Senkevich, T. G., C. L. White, E. V. Koonin, and B. Moss. 2000. A viral member of the ERV1/ALR protein family participates in a cytoplasmic pathway of disulfide bond formation. Proc. Natl. Acad. Sci. U. S. A. 97:12068–12073.
47. Shavinskaya, A., S. Boulant, F. Penin, J. McLauchlan, and R. Bartenschlager. 2007. The lipid droplet binding domain of hepatitis C virus core protein is a major determinant for efficient virus assembly. J. Biol. Chem. 282:37158–37169.
48. Shimakami, T., R. E. Lanford, and S. M. Lemon. 2009. Hepatitis C: recent successes and continuing challenges in the development of improved treatment modalities. Curr. Opin. Pharmacol. 9:537–544.
49. Tellinghuisen, T. L., M. J. Evans, T. von Hahn, S. You, and C. M. Rice. 2007. Studying hepatitis C virus: making the best of a bad virus. J. Virol. 81:8853–8867.
50. Tellinghuisen, T. L., and C. M. Rice. 2002. Interaction between hepatitis C virus proteins and host cell factors. Curr. Opin. Microbiol. 5:419–427.
51. Thompson, A. J., and J. G. McHutchison. 2009. Antiviral resistance and specifically targeted therapy for HCV (STAT-C). J. Viral Hepat. 16:377–387.
52. Tscherne, D. M., C. T. Jones, M. J. Evans, B. D. Lindenbach, J. A. McKeating, and C. M. Rice. 2006. Time- and temperature-dependent activation of hepatitis C virus for low-pH-triggered entry. J. Virol. 80:1734–1741.
53. Wakita, T., T. Pietschmann, T. Kato, T. Date, M. Miyamoto, Z. Zhao, K. Murthy, A. Habermann, H. G. Krausslich, M. Mizokami, R. Bartenschlager, and T. J. Liang. 2005. Production of infectious hepatitis C virus in tissue culture from a cloned viral genome. Nat. Med. 11:791–796.
54. Wootton, S. K., and D. Yoo. 2003. Homo-oligomerization of the porcine reproductive and respiratory syndrome virus nucleocapsid protein and the role of disulfide linkages. J. Virol. 77:4546–4557.
55. Zhou, S., and D. N. Standring. 1992. Cys residues of the hepatitis B virus capsid protein are not essential for the assembly of viral core particles but can influence their stability. J. Virol. 66:5393–5398.
56. Zhou, S., and D. N. Standring. 1992. Hepatitis B virus capsid particles are assembled from core-protein dimer precursors. Proc. Natl. Acad. Sci. U. S. A. 89:10046–10050.
57. Zweig, M., C. J. Heilman, Jr., and B. Hampar. 1979. Identification of disulfide-linked protein complexes in the nucleocapsids of herpes simplex virus type 2. Virology 94:442–450.